IVYSPRING INTERNATIONAL PUBLISHER

Theranostics

2023; 13(11): 3707-3724. doi: 10.7150/thno.81981

Research Paper

Extracellular vesicles improve GABAergic transmission in Huntington's disease iPSC-derived neurons

Margarida Beatriz[1,2], Ricardo J. Rodrigues[1,2], Rita Vilaça[1,2], Conceição Egas[1,2,3], Paulo S. Pinheiro[1,4], George Q. Daley[5,6], Thorsten M. Schlaeger[5,6], Nuno Raimundo[7], A. Cristina Rego[1,8]✉, Carla Lopes[1,2,7]✉

1. CNC - Center for Neuroscience and Cell Biology, CIBB - Centre for Innovative Biomedicine and Biotechnology, University of Coimbra, Coimbra, Portugal.
2. IIIUC - Institute for Interdisciplinary Research, University of Coimbra, Coimbra, Portugal.
3. Biocant- Transfer Technology Association, Biocant Park, Cantanhede, Portugal.
4. Faculty of Sciences and Technology, Department of Life Sciences, University of Coimbra, 3000-456 Coimbra, Portugal.
5. Division of Pediatric Hematology/Oncology, Children's Hospital Boston, Boston, MA USA.
6. Harvard Stem Cell Institute, Boston, MA USA.
7. MIA - Multidisciplinary Institute of Ageing, University of Coimbra, Coimbra, Portugal.
8. FMUC - Faculty of Medicine, University of Coimbra, Coimbra, Portugal.

✉ Corresponding authors: Carla Lopes, Ph.D., CNC-Center for Neuroscience and Cell Biology, University of Coimbra, Coimbra, Portugal. **Email:** clopes@uc.pt; carlalopes09@gmail.com. Ana Cristina Carvalho Rego, Ph.D., Center for Neuroscience and Cell Biology, and Faculty of Medicine, University of Coimbra, Coimbra, Portugal. **Email:** acrego@cnc.uc.pt; arego@fmed.uc.pt.

Received: 2022.12.19; Accepted: 2023.05.22; Published: 2023.06.26

Abstract

Background: Extracellular vesicles (EVs) carry bioactive molecules associated with various biological processes, including miRNAs. In both Huntington's disease (HD) models and human samples, altered expression of miRNAs involved in synapse regulation was reported. Recently, the use of EV cargo to reverse phenotypic alterations in disease models with synaptopathy as the end result of the pathophysiological cascade has become an interesting possibility.

Methods: Here, we assessed the contribution of EVs to GABAergic synaptic alterations using a human HD model and studied the miRNA content of isolated EVs.

Results: After differentiating human induced pluripotent stem cells into electrophysiologically active striatal-like GABAergic neurons, we found that HD-derived neurons displayed reduced density of inhibitory synapse markers and GABA receptor-mediated ionotropic signaling. Treatment with EVs secreted by control (CTR) fibroblasts reversed the deficits in GABAergic synaptic transmission and increased the density of inhibitory synapses in HD-derived neuron cultures, while EVs from HD-derived fibroblasts had the opposite effects on CTR-derived neurons. Moreover, analysis of miRNAs from purified EVs identified a set of differentially expressed miRNAs between manifest HD, premanifest, and CTR lines with predicted synaptic targets.

Conclusion: The EV-mediated reversal of the abnormal GABAergic phenotype in HD-derived neurons reinforces the potential role of EV-miRNAs on synapse regulation.

Keywords: Extracellular vesicles, Huntington's disease, synaptogenesis, miRNAs

Introduction

Huntington's disease (HD) is an autosomal dominant disorder associated with the expansion of a CAG triplet in exon 1 of the *huntingtin* gene [1]. The translated mutant huntingtin (mHTT) has an expanded polyglutamine stretch that causes conformational changes, abnormal protein interactions, and aggregation [2]. The primary disease hallmark is a selective loss of striatal medium spiny neurons (MSNs), with symptoms including neuropsychiatric signs and cognitive deficits that can precede motor symptom onset by over 15 years [3-5]. Indeed, neuroimaging studies show that striatal connectivity is altered before clinical diagnosis [6, 7].

Gamma-aminobutyric acid (GABA)-ergic MSNs,

the most common striatal neurons, receive glutamatergic projections from the cortex and their loss typically coexists with loss of cortical pyramidal neurons, primarily in motor and premotor areas [8, 9]. Dysregulation of GABAergic signaling significantly contributes to HD pathogenesis, especially $GABA_A$ receptor-mediated signaling, which is altered in the brains of several HD mouse models and human patients [10]. MHTT interacts with different organelles and proteins, particularly at synapses, affecting their normal function and ultimately resulting in degeneration [11-15]. Both wild type (WT) and mutant forms of huntingtin (HTT) were shown to interact with KCC2, a Cl^- cotransporter that promotes GABAergic inhibitory signaling, with a decrease in its expression leading to an over-excitation in the hippocampus of an HD mouse model [11]. Additionally, mHTT disrupts the translocation of $GABA_A$ receptors to the synapse by interfering with the affinity of HTT-associated protein 1 for KIF5, a kinesin motor protein [14, 15]. The interaction between mHTT and the SorCS2 protein, which regulates the trafficking of the subunit 2A of NMDA receptors in MSNs, leads to motor deficits in a HD mouse model [13]. Furthermore, the dendritic transport of TrkB receptors, that mediate brain-derived neurotrophic factor (BDNF) signaling, is compromised by mHTT, causing diminished activity of the ERK pathway in HD striatal neurons [12]. Moreover, a decrease in GABA content and GABAergic function were measured in the *substantia nigra* of postmortem brain samples of HD patients and the striatum of HD carriers through PET analysis [16, 17], as well as decreased mRNA and protein levels of $GABA_AR$ α1 and β2 subunits in the external globus pallidus of HD mouse models [15, 18]. Finally, gephyrin, a scaffold protein present in inhibitory post-synapses, was also decreased in a HD mouse model, along with the diminished frequency of miniature inhibitory postsynaptic currents (mIPSC) and GABAergic synapse density [18]. Therefore, mHTT can likely act as a disruptor of GABAergic synaptic activity and, thus, restoring normal GABAergic function could constitute a therapeutic opportunity in HD.

Extracellular vesicles (EVs) are nanosized structures that act as intercellular messengers containing different bioactive cargoes, such as lipids, proteins, DNA, and miRNAs [19]. Recently, the role of miRNAs associated with EVs has been explored in several neurodegenerative diseases, either as biomarkers or as modulators of the underlying pathological processes [20]. MiRNAs are small, non-coding RNAs that exert a modulatory effect on mRNA translation that helps maintain the balance of numerous neuronal mechanisms, including the formation, maturation, and function of synapses [21]. The expression of several miRNAs that modulate synaptic function and maturation is altered in the cortex and striatum of HD mouse models [22, 23], leading to changes in the levels of their predicted gene. One of the downregulated miRNAs is miR-132, involved in the regulation of methyl-CpG binding protein 2 (MeCP2) gene expression that was suggested to abnormally interact with mHTT and cause transcriptional dysregulation [22]. *MeCP2* is an important regulator of synaptic plasticity and homeostasis, and loss- or gain-of-function mutations trigger opposite changes in synaptic transmission [23]. MiR-200a and miR-200c are also found altered in HD [24] and their targets include *neurexin 1,* which is important to maintain synaptic function in the striatal circuitry [25]. Importantly, in postmortem HD brains, cerebrospinal fluid, and plasma, various miRNAs are found altered, including some that are critical for neuronal function [26-28]. Therefore, because dysregulated miRNAs may play important roles in HD pathogenesis, a miRNA-based therapeutic strategy could be effective.

An approach with observed effects in counterbalancing pathological alterations is the use of EVs. While the treatment with EVs in HD models has mainly resulted in the observation of reduced mHTT aggregates and increased neuronal survival [29-31], studies regarding other pathological conditions reported effects of EV administration on synaptic transmission [32-35]. In this work, EVs secreted from fibroblasts of HD patients previously characterized according to disease stage [19] were used to treat human-derived striatal-like neurons. After treating human-derived HD striatal-like neurons with EVs secreted by CTR fibroblasts, we observed improvements in neuronal GABAergic signaling. Contrarily, EVs secreted by HD-derived fibroblasts generated the opposite outcome on CTR-neurons, suggesting a role for EVs in the propagation of cellular toxic effects and influencing neuronal function. Moreover, we observed divergent miRNA profiles in HD- and CTR-EVs, evidencing that EV-miRNAs may play a role as regulators of synaptic-related proteins and be involved in HD pathology.

Materials and Methods

Cell culture and reagents

Human dermal fibroblasts were obtained from skin punches of HD patients (mutant HTT gene carriers) and from healthy control individuals (CTR), as described previously [36]. A total of nine lines of fibroblasts were used: three CTR lines (fCTR1, fCTR2, fCTR3), three from premanifest HD patients (fpHD1, fpHD2, fpHD3), and three from manifest HD patients

(fHD1, fHD2, fHD3). Fibroblasts were grown in DMEM medium (#D5648, Gibco) supplemented with 9 mM sodium bicarbonate, 10% fetal bovine serum (FBS; Gibco) and 1% penicillin/streptomycin (Gibco). Induced pluripotent stem cells (iPSCs) were reprogrammed from human dermal fibroblasts (from two HD carrier-derived lines with 43 [fHD3] and 46 [fHD1] CAG repeats and two CTR lines [fCTR1, fCTR3]; Figure 1D) [19]. iPSCs were maintained in Geltrex®-coated plates with StemFlex medium (Gibco). Differentiation into a striatal-specific neuronal phenotype was performed as previously described [19]. Briefly, neuronal induction medium was supplemented with 5 µM Dorsomorphin (Sigma) and 10 µM SB431542 (Peprotech) until day five and later 1 µM XAV 939 (Peprotech) and 200 ng/ml Sonic Hedgehog (SHH C-25II; R&D) were added until day 12 [37-39]. Neuronal progenitors were then dissociated with Accutase (GRiSP) and plated on Geltrex®-coated coverslips in 24-well plates for further neuronal differentiation using N2/B27 medium supplemented with 200 ng/ml SHH, 1µM XAV939 and 30 ng/ml brain-derived neurotrophic factor (BDNF; Peprotech) until day 26. From this point, the medium was changed every three days and only supplemented with 50 ng/ml BDNF to obtain striatal-like neurons at day 80. Cells were maintained in a humidified incubator at 37 °C with 5% CO_2.

Immunocytochemistry and image processing

Cells were washed with pre-warmed phosphate-buffered saline (PBS) at 37 °C, permeabilized using PHEM buffer (containing: 60 mM PIPES, 25 mM HEPES, 10 mM EGTA, and 2 mM $MgCl_2$, at pH 6.9) with 0.1% Triton® X-100 and fixed with PHEM/4% paraformaldehyde for 20 min. Blocking was performed for 40 min using PHEM with 0.1% Triton and 3% bovine serum albumin (BSA). Cells were incubated overnight at 4 °C with the following primary antibodies diluted in PHEM/0.1% Triton/3% BSA: anti-NANOG (D73G4; 1:200, #mAb 4903, Cell Signaling), anti-OCT4 (1:200, #2750, Cell Signaling), anti-Nestin (1:200; #MAB1259 R&D), anti-SOX2 (D9B8N; 1:200, #mAb 23064, Cell Signaling), anti-GAD 65/67 (1:100, #ab1511, Merck), anti-DARPP32 (EP720Y; 1:200, #ab40801, Abcam), anti-NeuN (1:500, #MAB377, Chemicon), anti-MAP2 (1:500, #ab92434, Abcam), anti-βIII-tubulin (1:200, #NB100-1612, Novus Biologicals), anti-VGlut1 (1:500, #135 307, Synaptic Systems), anti-SMI-32 (1:500, #837904, BioLegend), anti-Synaptophysin (1:500, #ab32127, Abcam), anti-Gephyrin (1:200, #147111, Synaptic Systems), anti-PSD95 (1:200, #51-6900, Thermofisher), anti-GABA1aR1 (1:50, #224 203, Synaptic Systems) and anti-GFAP (1:500, #AB5804, Chemicon). Cells were washed three times with PBS and further incubated with secondary antibodies diluted in PHEM/0.1% Triton/3% BSA (1:200) for one hour at room temperature (RT) and then washed three times (with a first quick wash and the following two washes for 10 min each) with PBS. The coverslips were mounted on glass slides using Mowiol (Sigma); Hoechst (1:10 000; Invitrogen) was used to stain the nuclei. Images were acquired on a Zeiss LSM 710 Confocal System (Carl Zeiss Microscopy) with 20x and 40x objectives. Colocalization studies of βIII-tubulin with MAP2 were performed on Z-stacks using the JACoP ImageJ plugin [40] and synapse counting using the SynapCountJ ImageJ plugin [41].

CAG PCR and agarose gel electrophoresis

The CAG repeat number in each cell line was determined by PCR using primers for Exon 1 CAG region, as described previously [42]. Briefly, 30 ng of genomic DNA was used for PCR with Phusion® High-Fidelity DNA polymerase in Phusion® GC buffer supplemented with 1 M betaine. Amplicons were separated in 2 % agarose gels with Tris/Borate/EDTA buffer and visualized with a Bio-Rad Gel Doc XR+ System. A small volume of the reaction was used for more accurate confirmation of the CAG number with an Agilent BioAnalyzer. Primers: HttCAG Fw: 5′-ATG GCG ACC CTG GAA AAG CTG AT-3′; HttCAG Rev: 5′-GGC TGA GGC AGC AGC GGC TG-3′.

Electrophysiological recordings

Whole-cell patch-clamp recordings were performed with an AxoPatch 200B amplifier (Molecular Devices) using borosilicate glass micropipettes with a resistance of 4–6 MΩ. The voltage-clamp recordings of miniature inhibitory postsynaptic currents (mIPSCs) mediated by $GABA_AR$ were performed at a holding potential of -70 mV using an internal solution containing the following (in mM): CsCl 130, NaCl 10, EGTA 5, HEPES 10, $CaCl_2$ 0.5, MgATP 4, NaGTP 0.3, QX314 1 (pH 7.4 with CsOH). The extracellular solution contained the following (in mM): NaCl 140, KCl 2.5, $CaCl_2$ 2, $MgCl_2$ 1, HEPES 10 and glucose 15 (pH 7.4) plus 1 µM tetrodotoxin, 20 µM CNQX and 5 µM 5,7-DiCl-kynurenic acid (Tocris, UK). For whole-cell $GABA_AR$-mediated currents, GABA (100 µM), daily prepared in extracellular solution, was rapidly applied to cells with a perfusion valve control system VC-77SP/perfusion fast-step SF-77B (Warner Instruments, USA). Both the voltage-clamp whole-cell current recordings and the current-clamp recordings were performed using an internal solution containing the following (in mM): K-gluconate 130, NaCl 4, $MgCl_2$ 2, EGTA 1, HEPES 10, phosphocreatine 5,

Na_2-ATP 2 and Na_2-GTP 0.3 (pH 7.2 with KOH). The bathing solution contained the following (in mM): NaCl 140, KCl 3, $CaCl_2$ 2, $MgCl_2$ 1, HEPES 10, and glucose 15 (pH 7.4). All experiments were performed at RT (22–25 °C). The currents were filtered at 1–10 kHz, digitized at a sampling rate of 1-20 kHz to a personal computer, and analyzed with pClamp software (AXON Instruments, USA).

Isolation and characterization of EVs

Isolation of EVs was performed as previously described [19]. Briefly, fibroblasts were cultured in a medium depleted of EVs by centrifuging the FBS at 100 000 x*g* for 18 hours at 4 °C. Cell culture supernatant was collected from fibroblasts every 48 hours and stored at -80 °C for posterior use. For isolation of EVs, the culture media was filtered (0.22 µm) to remove cell debris, centrifuged at 10 000 *g* for 30 min, and then twice at 100 000 *g* for 70 min to pellet EVs [43]. EVs were resuspended in different buffers depending on the final use: PBS for RNA extraction, Nanosight tracking analysis (NTA) and incubations of neurons; PBS/2% paraformaldehyde for transmission electron microscopy (TEM) and RIPA for western blotting.

TEM and immunogold-TEM

The antibodies anti-1C2, which detects expanded polyglutamine (1:150, #MAB1574, Millipore), and anti-HTT (1:150, #MAB2166, Millipore), were used for immunoelectron labeling of isolated EVs. Briefly, EV samples were placed on carbon-Formvar-coated 300 mesh nickel grids, and samples were allowed to adsorb for 20 min. Following washing in PBS (2x 3 min), grids were floated (sample side down) onto 50 µl drops of 50 mM glycine (4x 3 min) to quench free aldehyde groups and then transferred to blocking solution (5% BSA, 0.01% saponin in PBS) for 10 min. Then, grids were incubated in blocking buffer (1% BSA, 0.01% saponin in PBS; negative control) or primary antibodies for two hours, followed by washing steps in PBS with 1% BSA (6x 3 min). Secondary antibodies (anti-mouse or anti-rabbit IgC immunogold conjugates, 1:200) were then added for one hour, followed by additional washing steps (8x 2 min), fixation in 1% glutaraldehyde for five min and washed in water (8x 2 min). A final contrasting step was performed using uranyl oxalate solution, pH 7.0, for five min, followed by a mixture of 4% uranyl acetate and 2% methylcellulose, for 10 min on ice. Imaging was conducted using a FEI-Tecnai G2 Spirit Bio Twin TEM at 100 kV.

Particle size and concentration analysis

EVs were resuspended in 1 ml of water containing low mineral concentration. Nanosight tracking analysis was performed in a NanoSight NS300 instrument with an sCMOS camera module (Malvern Panalytical). Analysis settings were optimized and kept constant between samples. For each sample, five videos were recorded and analyzed to obtain the mean size and estimated concentration of particles. Data were processed using the NTA 3.1 analysis software.

Western blotting

As previously described [44], cells were lysed in a lysis buffer (50 mM Tris-HCl pH 7.4, 150 mM NaCl, 1 mM EDTA, 1% TritonX-100) supplemented with a protease inhibitor cocktail (Sigma), and protein was quantified using the Bio-Rad Protein Assay (Bio-Rad). For protein denaturation, SDS sample buffer (50 mM Tris-HCl pH 6.8, 2% SDS, 5% glycerol, 600 mM DTT, 0.01% bromophenol blue) was added to protein lysates (30 µg for fibroblasts) and heated for five min at 95 °C. For EVs, the final isolated pellet (from 150 ml of fibroblast culture medium) was lysed in RIPA buffer and the protein was denatured in SDS sample buffer (non-reducing conditions were used to assess CD63 presence). Samples were then separated on 10-12% polyacrylamide gels and transferred onto methanol-activated polyvinylidene difluoride (PVDF) Hybond-P membranes (Millipore). Membranes were blocked in Tris-buffered saline with 0.1% Tween-20 (TBS-T) containing 5% BSA for one hour at RT and incubated overnight at 4 °C with anti-flotillin-2 (C42A3; 1:500, #3436, Cell Signaling), anti-calnexin (1:500, #ab10286, Abcam) and anti-CD63 (TS63; 1:500, #10628D, Life Technologies) diluted in TBS-T/1% BSA. Primary antibodies were washed with TBS-T and membranes were incubated with secondary antibodies anti-mouse and anti-rabbit coupled to alkaline phosphatase (1:5000; Sigma) diluted in TBS-T/1% BSA for one hour at RT. Secondary antibodies were washed with TBS-T, and immunoreactive bands were developed with ECF reagent (GE Healthcare) and imaged in a Chemidoc Imaging System (Bio-Rad).

Incubation of striatal-like neurons with EVs

EVs isolated from fibroblasts (fCTR3 and fpHD3) were diluted in PBS, quantified, and filtered (0.22 µm) as described above, before being added to neuronal culture media. Approximately, 2.0×10^7 EVs were added per well in each incubation [45]. HD striatal-like neurons were incubated with CTR-EVs and CTR striatal-like neurons with HD-EVs. EVs were added to the culture medium every other day for the last 5 days of differentiation (endpoint 80 days) [46]. Immunocytochemistry and electrophysiological recordings were made on day 80.

Plasmids and viral production

pCL6EGwo and pCL6-CD63eGFP plasmids were a kind gift from Dr. Helmut Hanenberg and Dr. Bernd Giebel (University of Duisburg-Essen, Germany), respectively. High-titer lentiviral particles were produced in HEK293T cells by transiently co-transfecting the described plasmids with psPAX2 (#12260, Addgene) and pCMV-VSV-G (#8454, Addgene) plasmids using the JetPrime reagent (Polyplus-transfection). After 48 hours, the viral particles were collected from the medium, purified, and concentrated as described previously [47]. Lentiviral titer was estimated using FACS based on an encoded fluorescent marker.

Small RNA Sequencing and Analysis

Library preparation and sequencing

Small RNA and miRNA quantity and quality in the nine EV samples were assessed by capillary electrophoresis in the 2100 Bioanalyzer and the Agilent Small RNA kit (Agilent Technologies). miRNA libraries were generated with the NEXTFLEX Small RNA Sequencing Kit v3® (Bioo Scientific Corp., 2019) from 3-20 ng of small RNA for each sample. NEXTFLEX 3′ 4N Adenylated adapter and NEXTFLEX 5′ 4N Adenylated adapter were diluted 1:4 as recommended for low input library preparation. NEXTFLEX tRNA/YRNA Blockers (Bioo Scientific, Perkin Elmer, Waltham, MA) were applied to deplete the tRNA and YRNA fragments. To increase yield, the 3′ adapter ligation was performed at 20ºC, overnight. First Strand cDNA synthesis was obtained by reverse transcription for 30 min at 42ºC, followed by 10 min at 90 ºC. Second Strand cDNA was obtained by PCR amplification for 25 cycles, with a Universal and a barcoded primer (one for each sample), included in the NEXTFLEX Small RNA Sequencing Kit v3. A PAGE-based size selection method was used for obtaining a purified ~150bp miRNA library. All library preparation procedures were carried out according to the manufacturer's instructions. Sequencing was performed at Genoinseq (Cantanhede, Portugal) on a NextSeq 550 Illumina sequencer with the NextSeq 500/550 MID Output (150 cycles) v2.5 kit (Illumina).

Data processing

Sequence data was processed at Genoinseq (Cantanhede, Portugal). Raw single-end reads (R1) were extracted from Illumina Nextseq® System in fastq format and quality-filtered with Trimmomatic version 0.3 [48] and Prinseq version 0.20.4 [49] to clip the NEXTFLEX Small RNA Sequencing Kit adapter and the first and last 4 N bases introduced during library preparation and to remove reads shorter than 18 bp. Ribosomal and transfer RNA reads were removed from the high-quality data by alignment against the RFam version 14.5 [50] using Bowtie version 1.0.0 [51]. The miRDeep2 package version 2.0.1.3 [52] was used to profile known miRNA expression in the 9 samples. The cleaned sequencing data were mapped against the human reference genome assembly GRCh37 (hg19) with Bowtie version 1.0.0, using default parameters and without mismatches. Then, the mapped reads were aligned against the miRBase version 22 [53], filtered for human miRNAs only, to identify and quantify all known mature miRNAs and their precursor sequences, also without allowing mismatches. miRDeep2 was also used to predict novel miRNAs from unannotated reads. The sequencing, filtering, and alignment metrics are presented in Supplementary Table S1.

EVs miRNA target prediction and pathway enrichment analysis

miRNA raw read counts were divided by the total count of their sample for normalization. To identify differentially expressed miRNAs we applied an FDR-adjusted p-value ($q \leq 0.05$) and fold changes ($\log2FC \geq |2.0|$). Fold-change was defined as the ratio (log2) between the average expression of the three samples for each pair of the analyzed conditions (CTR, pHD, and HD). miRDB- MicroRNA Target Prediction Database (http://mirdb.org/) was used to retrieve the EV miRNA gene targets [54]. Gene Ontology (GO) enrichment analyses for candidate miRNA targets were performed using the online Web-based tool NetworkAnalyst (https://www.networkanalyst.ca/) [55, 56]. NetworkAnalyst supports enrichment analysis with gene sets from the Gene Ontology and PANTHER, among other databases. SynGo was used to analyze the brain-expressed genes (https://syngoportal.org/) [57]. The gene ontology enrichment analysis was performed for the category GABAergic synapse (GO:0098982). A normalized average gene expression of SynGO genes (release 20210225-1.1) in GABAergic neurons obtained from a total number of 177614 GABAergic cells and of 1205 SynGO genes in the dataset, kindly provided by Dr. Verhage and Dr. Roig Adam, was used. Principal Component Analysis (PCA) plots and heatmaps were performed in the web tool ClustVis (https://biit.cs.ut.ee/clustvis/) [58]. Venn diagrams were made at https://bioinformatics.psb.ugent.be/webtools/Venn/.

Statistical analysis

Statistical computations were performed using GraphPad Prism version 9.0 (GraphPad Software, La

Jolla, CA, USA), and SPSS version 21.0 (IBM SPSS Statistics for Windows, IBM Corp). Results are represented as the mean ± SEM of the indicated number of independent experiments in the figure legends. For cell experiments, at least three independent assays were performed for each experimental condition. Statistical significance was analyzed using the parametric test one-way ANOVA followed by Bonferroni post hoc test and non-parametric test Kruskal Wallis followed by Dunn's multiple comparison test. Correlations were done using the Spearman rank correlation coefficient (ρ). $p < 0.05$ or q (p-adjusted) < 0.05 was considered statistically significant.

Results

Differentiation and maturation of striatal-like neurons

In this study, we used a previously published protocol [19, 38] to promote neural induction in pluripotent cell colonies and obtain mature neurons (Figure S1A). Pluripotency (Nanog and OCT4) and neural induction (Nestin) markers were assessed in iPSCs and NSCs, respectively (Figure 1A). During the differentiation protocol, cells were characterized for the presence of markers of GABAergic (GAD 65/67$^+$) and MSN (DARPP32$^+$) development, and for commitment to a mature neuronal fate by assessing βIII-tubulin$^+$ and MAP2$^+$ cell populations on days 45 and 60 of differentiation (Figure 1B). The HD cell lines have the capacity to mature at the appropriate time course. Dense clusters of βIII-tubulin$^+$ and MAP2$^+$ cells are present after 60 days of differentiation, despite an increase in βIII-tubulin$^+$ reactivity in HD cells (Figure 1B). Furthermore, when analyzing the expression of DARPP32 to identify the capacity for terminal maturation into MSNs, the HD-derived neuronal cultures show a reduction over time (from 45 to 60 days) compared to CTR neurons (Figure 1B). By day 80, the majority of differentiated cells expressed the axonal marker SMI-312, but very few neurons were immunoreactive for VGlut1 (Figure 1C). To assess the successful establishment of inhibitory synapses, we measured inhibitory synapse density based on the colocalization of the general

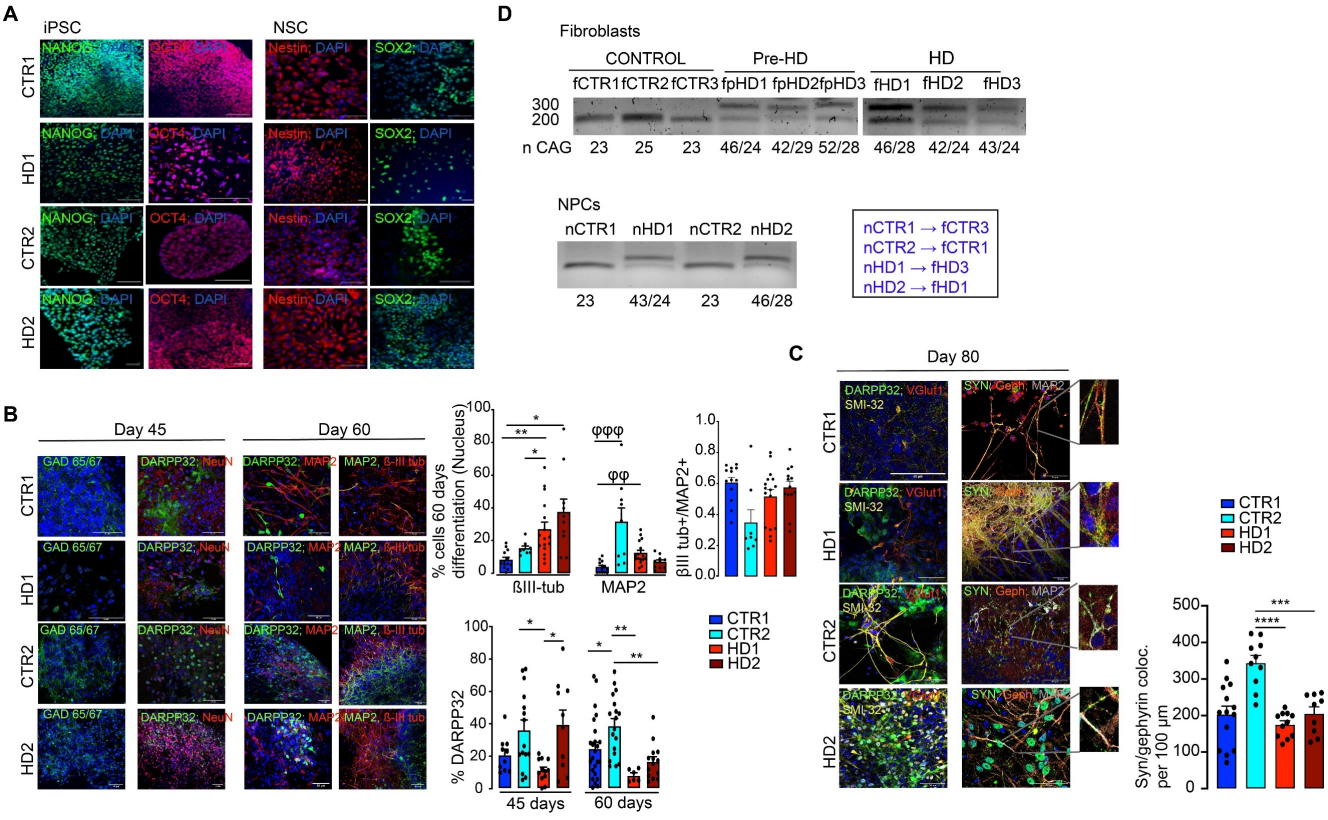

Figure 1. Phenotypic characterization of striatal progenitors and neurons generated from human CTR and HD iPSCs. (A) IPSCs and differentiated NSCs exhibit pluripotency and neural progenitor markers (Nanog and OCT4; Nestin and SOX2) (scale bar, 20 µm (B) Neural progenitors express a GABAergic synaptic marker (GAD 65/67) and neuronal (βIII-tubulin, MAP2, and NeuN) and striatal (DARPP32) specific markers (n > 13). βIII-tubulin and MAP2 levels at 60 days and DARPP32$^+$ cells during neuronal differentiation at 45 and 60 days (n > 10). (C) Differentiated neurons express markers for GABAergic neurons (DARPP32 and SMI-32$^+$) and show colocalization of the pre- and postsynaptic markers synaptophysin (SYN) and gephyrin (Geph), showing inhibitory synapse formation (n > 9). (D) CAG repeat sizes for the wild-type (lower band) and mutant alleles (upper band) in fibroblasts and NSCs. Correspondence between patient fibroblasts and differentiated NSCs is also indicated. Bar plots represent mean ± SEM. One-way ANOVA followed by Tukey's multiple comparisons test: * $p < 0.05$, ** $p < 0.01$, *** $p < 0.001$, **** $p < 0.0001$; or Kruskalis-Wallis followed by Dunn's multiple comparisons test: ϕϕϕ $p < 0.001$, ϕϕ $p < 0.01$.

presynaptic protein, synaptophysin, with the inhibitory postsynaptic protein Gephyrin. We found that synapse density was decreased in HD striatal-like neurons compared to CTR2 (Figure 1C). We also assessed excitatory synapse density through the colocalization of synaptophysin with the excitatory postsynaptic protein PSD-95 and found it to be decreased in HD1 neurons compared to CTR2 and in HD2 compared to both CTRs (Figure S1B). In addition, we observed the presence of a GFAP$^+$ glial population of cells (Figure S1C). The abnormal CAG expansion in HD-derived cells was confirmed by PCR (Figure 1D). Together, these data demonstrate that HD-derived neurons show a potential delay in maturation into a MSN phenotype and display reduced inhibitory synapse density.

To further validate the delayed maturation from a functional perspective, the electrophysiological properties of differentiated HD and CTR neurons were analyzed through whole-cell current-clamp recordings. At day 60 of the differentiation protocol, neurons were still immature, and action potential firing capacity upon injection of depolarizing current pulses was low. However, at day 80, both HD- and CTR-derived neurons could reliably generate action potentials in response to depolarizing current injections, exhibiting single and repetitive spiking, indicating similar levels of maturation (Figure 2A). The mean resting membrane potential of HD striatal-like neurons was shifted toward more positive values (HD1: -42.2 ± 2.0 mV and HD2: -33.7 ± 2.0 mV) compared to CTRs (CTR1: -46.9 ± 1.9 mV and CTR2: -48.6 ± 1.6 mV) indicating that HD neurons are more depolarized, although only HD2 presented a statistically significant alteration compared to CTRs ($p < 0.05$). Nonetheless, the action potential threshold was the same between HD and CTR cells (Figure 2B). We also found that HD striatal-like neurons had a lower rheobase compared to CTR2 neurons, which reflects greater excitability (Figure 2B). In agreement with this, the HD2 cell line also exhibited a higher input resistance compared to the CTR neurons (Figure S2A). Since voltage-gated sodium (Na$^+$) and potassium (K$^+$) channels are essential players in neuronal

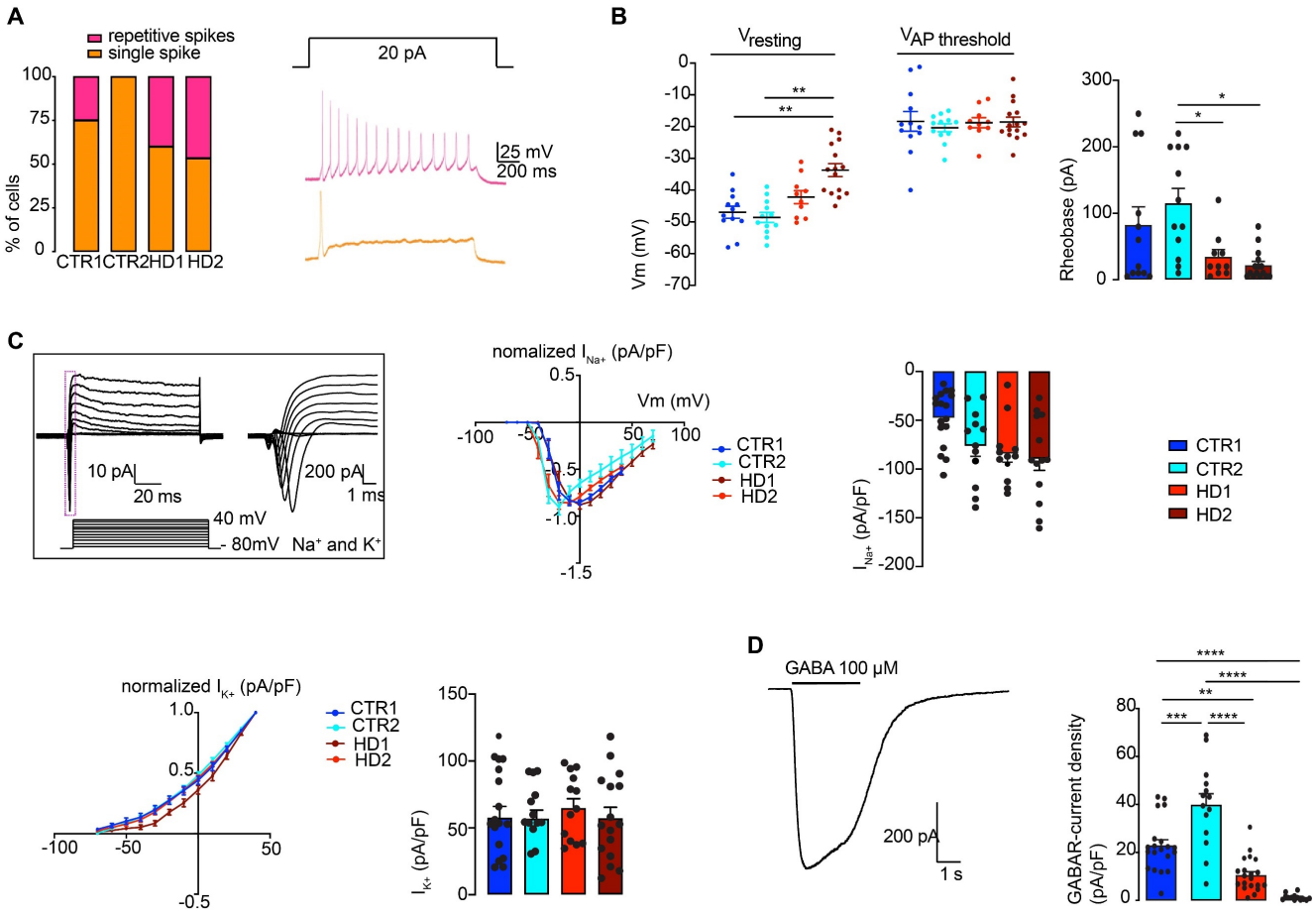

Figure 2. Electrophysiological characterization of mature striatal-like neurons. (A) Differentiated neurons can generate single or sustained action potentials in response to depolarizing current injections. B) HD-derived neurons have a less negative resting potential. C) HD-derived neurons display altered voltage-dependence of Na$^+$ and K$^+$ conductance. D) HD-derived neurons show reduced $GABA_A$ receptor-mediated currents in response to rapid application of GABA (100 µM). Bar plots represent mean ± SEM. One-way ANOVA followed by Tukey's multiple comparisons test: * $p < 0.05$, ** $p < 0.01$, *** $p < 0.001$, **** $p < 0.0001$.

physiology, we evaluated the activation of fast voltage-gated Na^+ and delayed-rectifier K^+ currents (Figure 2C). The normalized I/V curves for Na^+ suggest that the activation threshold is similar between CTR and HD neurons, despite the latter having a tendency for larger maximum current densities, probably due to differences in the membrane levels of Na^+ channels. The I/V curves for K^+ show a slight shift in activation toward a more positive potential in the HD2 cell line. No significant alterations were observed between HD and CTR neurons for maximum K^+ current density (Figure 2C).

Since we aimed to obtain an enriched population of GABAergic neurons, we further analyzed if functional $GABA_A$ receptors were expressed at the cell membrane by using a fast bath application of 100 µM GABA and measured the whole-cell $GABA_A$ receptor-mediated currents. The whole-cell $GABA_A$ receptor-mediated current density was significantly smaller in HD striatal-like neurons compared to CTRs (CTR1: 22.9 ± 2.4 pA/pF; CTR2: 39.8 ± 4.7 pA/pF; HD1: 10.4 ± 1.5 pA/pF and HD2: 1.3 ± 0.4 pA/pF; $p < 0.05$) (Figure 2D), indicative of an overall lower expression of GABA receptors. Collectively, these data show that differentiated neurons presented a MSN phenotype and that HD-derived neurons were more excitable and had a decreased $GABA_A$ receptor-mediated current density.

HD-derived neurons display a lower density of inhibitory synapses that is normalized upon incubation with EVs

It has been demonstrated that EVs carry miRNAs that are important for cell signaling pathways, including those known to promote synaptogenesis [59]. To evaluate the effects of EVs on mature striatal-like neurons, we first isolated small EVs and characterized them according to ISEV guidelines [60]. EVs were isolated from the cell culture media of human fibroblast lines from three CTR donors and six HD carriers (premanifest and manifest) [36] using a multi-step centrifugation protocol [43]. EVs presented the expected cap-shaped morphology when observed by TEM (Figure 3A) and a size range of 50-200 nm (Figure 3B) [60]. Small EV protein markers like Flotillin-2 and CD63 were present; the absence of Calnexin as a cellular contaminant validated the purity of the isolated pool of vesicles (Figure 3C). As shown previously [46, 61], we also detected the presence of both HTT and mHTT in EVs from fibroblasts of one CTR and two HD carriers (premanifest and manifest), respectively, by immunogold-TEM (Figure 3D).

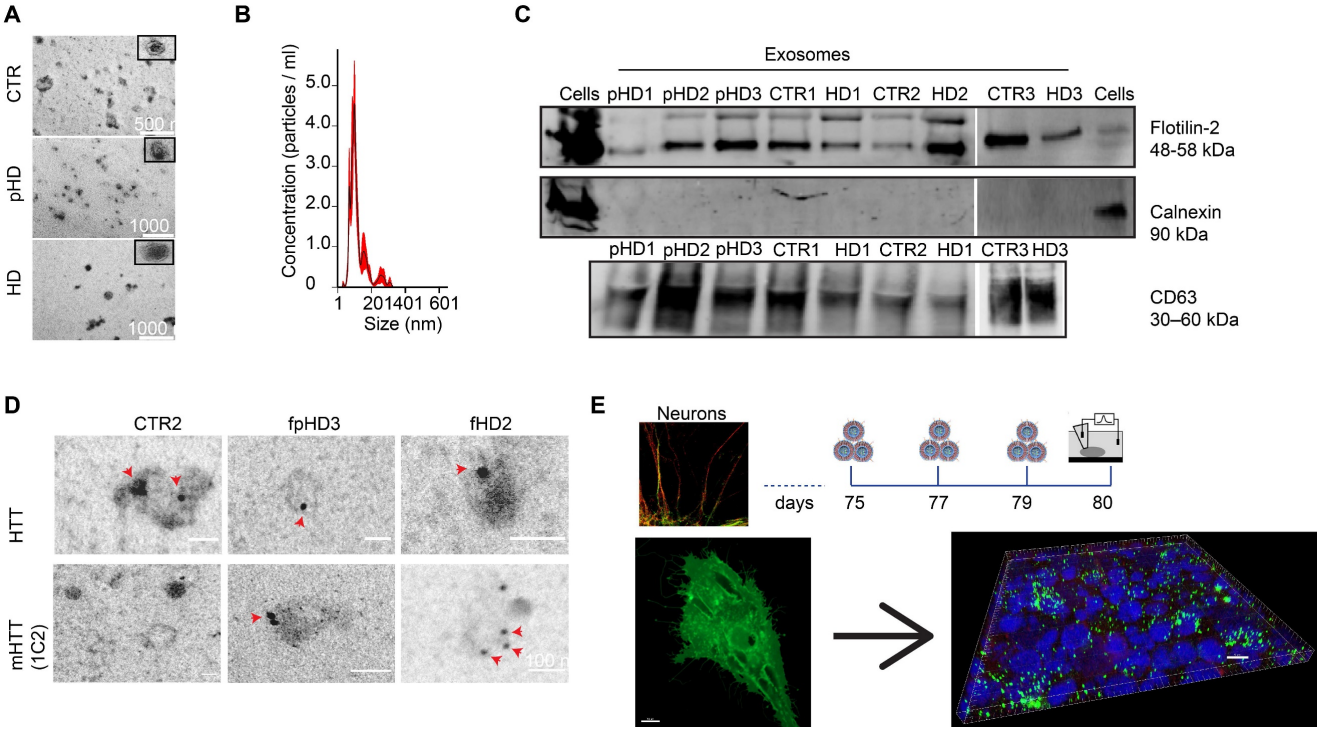

Figure 3. Characterization of fibroblast-derived EVs. (A) TEM images of fibroblast-derived EVs (scale bar: fCTR2, 500 nm; fpHD3 and fHD2, 1000 nm). (B) Representative analysis of NTA measurements of fibroblast EV concentration (particles/ml) and size (nm). (C) Representative Western blot with conventional EV markers in fibroblast EVs (Flotillin-2 and CD63) and Calnexin as a negative control for cellular contamination. (D) HTT and mHTT (1C2) immunogold labeling in fibroblast EVs (scale bar, 100 nm). (E) Timeline for incubation of differentiated CTR and HD neurons with EVs isolated from CD63+-GFP expressing fibroblasts followed by 3-D reconstruction with IMARIS software of the Z-stacks of confocal images (EVs, green; MAP2, red). Scale, 50 µm.

To assess the effects of EVs in differentiated striatal-like neurons, we applied an incubation protocol of fibroblast EVs (using EVs secreted from one CTR and one HD carrier fibroblast line) during the last five days of neuronal differentiation (Figure 3E) [45, 46]. EVs were added to neurons every other day until day 80 of differentiation. To confirm the uptake of EVs by neuronal cultures, we performed a parallel incubation of neuron cultures with EVs obtained from GFP-CD63-expressing fibroblasts. 3D reconstruction with IMARIS software shows EVs inside $MAP2^+$ neurons (Figure 3E). After incubation of HD-derived neurons with CTR-EVs for five days, a normalization in the GABAR-mediated current density was observed, whilst incubation of CTR-derived neurons with HD-EVs resulted in the opposite effect (Figure 4A).

Next, we assessed if, in addition to having surface $GABA_A$ receptors, the differentiated neurons also had synaptic $GABA_A$ receptor-mediated mIPSCs and whether these were influenced by treatment with EVs. HD-derived neuron lines had lower mIPSC frequency (higher inter-event intervals) that increased significantly after incubation with CTR-EVs, suggesting an increased number of active synaptic contacts. No differences were found in mIPSC amplitude between non-treated and EV-treated neurons, suggesting that the number of $GABA_A$ receptors at individual synapses was unchanged (Figure 4B). To confirm that EVs were causing an increase in the number of synaptic contacts, we quantified the colocalization of Synaptophysin with Gephyrin as a measure of GABAergic synapse density. In the HD-derived neurons treated with CTR-EVs, a significant increase in inhibitory synapse density was observed, while in CTR-derived neurons treated with HD-EVs the opposite effect occurred (Figure 4C, Figure S2). Therefore, while EVs secreted by CTR fibroblasts promote GABAergic synapse formation, EVs secreted by HD fibroblasts impair this process.

miRNAs targeting synaptic genes are enriched in EVs

To explore the hypothesis that miRNAs carried by EVs could be involved in their synaptogenic effect, we analyzed the miRNA profile of EVs released from the three CTR and six HD (three premanifest-pHD1, pHD2, pHD3- and three manifest- HD1, HD2, HD3) fibroblast lines used for the previous incubations. In total, 393 miRNAs were detected in EVs, and two distinct miRNA clusters could be observed after hierarchical grouping of the top 100 miRNAs (CTRs, pHDs, and HDs), although samples did not cluster distinctly according to their origin (Figure 5A). The principal component analysis (PCA) showed a clear distinction between EVs isolated from premanifest patients and CTRs, except for the CTR2 cell line (Figure 5B). When looking at miRNA composition, 227 miRNAs were detected across all group samples (Figure 5C, Supplementary Table S2). When analyzing only premanifest and manifest cell lines, we observed the smallest number of EV-associated miRNAs in common (8) when compared to premanifest vs CTR (20) or manifest vs CTR (32) (Figure 5D). Interestingly, some of the miRNAs were exclusively detected in a specific cell-derived EV population, confirming the selective incorporation of miRNAs into EVs (Figure 5C).

Since we could not identify differentially expressed miRNAs between samples (q-value < 0.05), probably due to the reduced sample size, we further analyzed the miRNAs by their fold change. From the upregulated miRNAs with logFC > 2, we found 28 for pHD vs CTR; 23 for HD vs CTR, and 18 for HD vs pHD. The downregulated miRNAs with logFC < -2 were less numerous: 12 for pHD vs CTR; 2 for HD vs CTR and 13 for HD vs pHD (Table 1, Supplementary Table S2). Among the most enriched miRNAs in EVs, hsa-miR-576-3p was upregulated in both HD and pHD vs CTRs, hsa-miR-1260a was found upregulated in HD and downregulated in pHD vs CTRs and hsa-miR-1260b was more abundant in HD-EVs than in the other groups (Table 1, Supplementary Table S2).

To identify the putative genes targeted by these miRNAs we used the online database miRDB, to predict the target genes of miRNAs that were up- or downregulated at least two-fold in our EV populations (Supplementary Table S2). The prediction results were sorted in descending order, as ranked by the target score, and only candidate transcripts with scores ≥ 60 are presented, to increase the prediction confidence (Supplementary Table S3).

We next performed a target enrichment analysis to identify cellular pathways or functional categories of the putative target genes. Interestingly, we observed an enrichment for targets in neuronal and synaptic components in both up- and downregulated miRNAs (Supplementary Table 4). Moreover, the target genes of the highly enriched miR-1260 family in HD-EVs included the cellular components "Neuronal cell body", "Dendrite", "Axon" and "Presynaptic membrane", showing they can potentially target neuronal activity. Also, the target genes of the upregulated hsa-miR-576-3p in the EVs from HD and pHD show an enrichment profile for the cellular components "Neuron projection" and "Axon" (Figure S3; Supplementary Table S4).

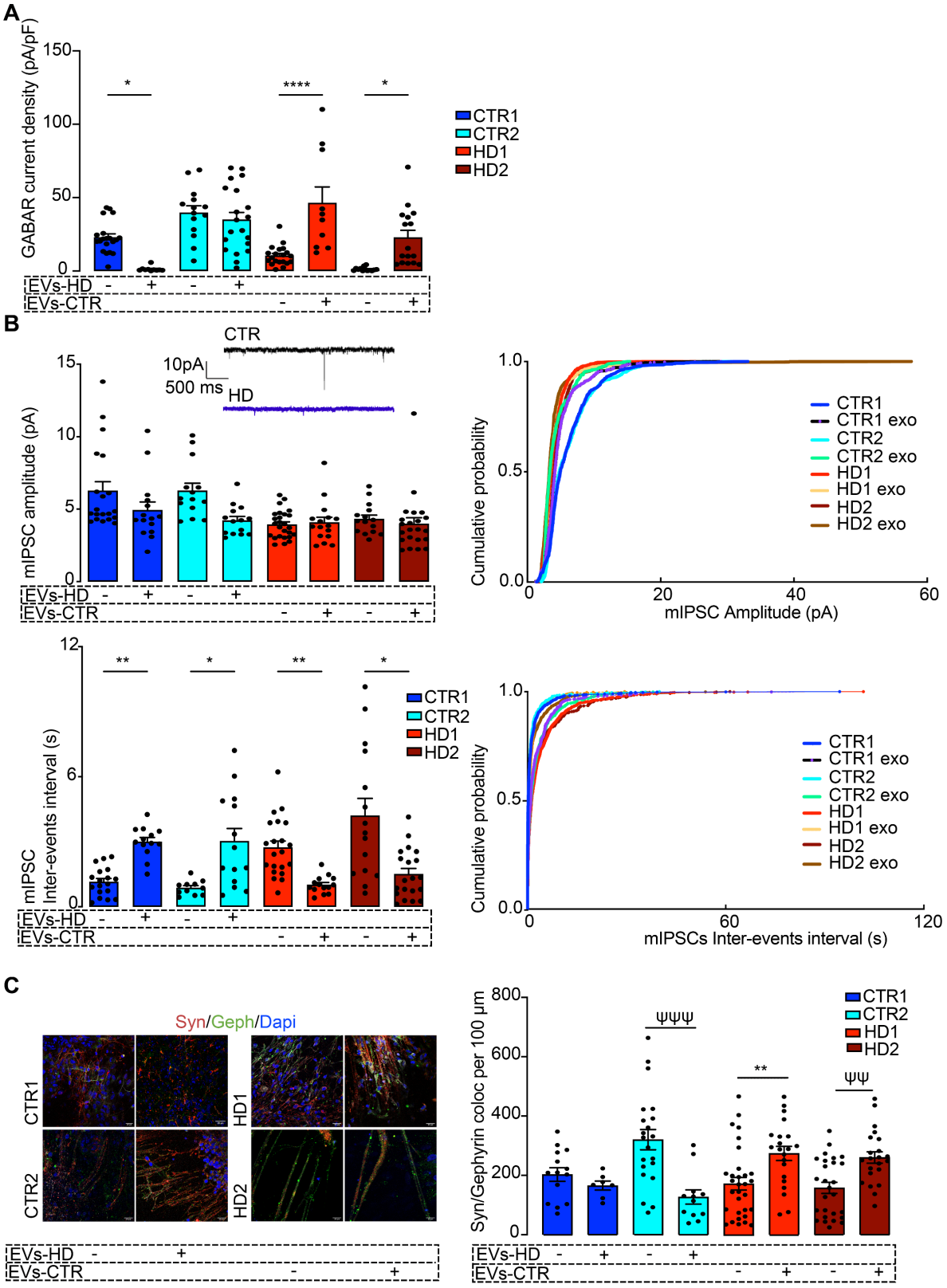

Figure 4. Fibroblast-derived EVs ameliorate the abnormal GABAergic function of human HD iPSC-Derived Neurons. (A) Reduced $GABA_A$ receptor-mediated currents in HD-derived neurons are rescued by incubation with EVs from CTR fibroblasts. (B) HD-derived neurons display reduced mIPSC amplitude and decreased miniature inhibitory postsynaptic current (mIPSC) frequency (increased inter-event interval), and incubation of HD-derived neurons with CTR-EVs recovered the frequency of events while the opposite effects occur in CTR-derived neurons incubated with HD-EVs. (C) Increased colocalization of synaptic markers (synaptophysin, red; gephyrin, green) in HD-derived neurons upon incubation with EVs from CTR fibroblasts, indicating enhanced synapse formation; the opposite effect was observed in CTR-derived neurons exposed to HD fibroblast EVs. Scale, 20 µm. Bar plots represent mean ± SEM. One-way ANOVA followed by Tukey's multiple comparisons test: * $p < 0.05$, ** $p < 0.01$, **** $p < 0.0001$; or Mann-Whitney test: ψψ $p < 0.01$, ψψψ $p < 0.001$.

Table 1. Up- and down-regulated microRNAs in fibroblast-derived EVs from patients with HD.

	upregulated			downregulated		
	miRNA	**FC**	**FDR q value**	**miRNA**	**FC**	**FDR q value**
pHD/CTR	hsa-miR-576-3p*	6,34	0,74	hsa-miR-1260a	-5,95	0,75
	hsa-miR-184	6,25	0,75	hsa-miR-19a-3p	-4,61	0,59
	hsa-miR-99a-3p	4,40	0,76	hsa-miR-30d-3p$	-3,90	0,73
	hsa-miR-34c-3p*	4,14	0,74	hsa-miR-590-3p	-2,95	0,74
	hsa-miR-210-3p	3,82	0,76	hsa-miR-26b-3p	-2,79	0,74
	hsa-miR-1277-3p*	3,70	0,76	hsa-miR-2355-3p	-2,56	0,74
	hsa-miR-377-3p	3,67	0,76	hsa-miR-18a-3p	-2,49	0,74
	hsa-miR-195-3p*	3,66	0,71	hsa-miR-598-3p	-2,44	0,74
	hsa-miR-1228-3p	3,54	0,74	hsa-miR-2110	-2,24	0,74
	hsa-miR-129-2-3p	3,51	0,74	hsa-miR-6529-3p	-2,17	0,74
	hsa-miR-4454*	3,46	0,74	hsa-miR-1180-3p	-2,15	0,75
	hsa-miR-548l*	3,40	0,76	hsa-miR-181a-3p	-2,12	0,74
	hsa-miR-204-3p	3,31	0,77			
	hsa-miR-940	2,83	0,74			
	hsa-miR-323b-3p*	2,59	0,78			
	hsa-miR-34a-3p*	2,41	0,78			
	hsa-miR-5010-3p	2,29	0,78			
	hsa-miR-324-3p	2,28	0,74			
	hsa-miR-3158-3p	2,27	0,78			
	hsa-miR-10401-3p	2,25	0,74			
	hsa-miR-1843	2,21	0,74			
	hsa-miR-1185-2-3p	2,21	0,78			
	hsa-miR-365a-3p*	2,18	0,74			
	hsa-miR-365b-3p*	2,18	0,74			
	hsa-let-7e-3p	2,13	0,74			
	hsa-miR-548w	2,11	0,74			
	hsa-miR-339-3p	2,05	0,74			
	hsa-miR-133a-3p	2,04	0,75			
HD/CTR	hsa-miR-576-3p	5,83	0,84	hsa-miR-30b-3p	-2,18	0,15
	hsa-miR-1260a#	5,48	0,85	hsa-miR-30d-3p $	-3,34	0,20
	hsa-miR-4429#	4,96	0,84			
	hsa-miR-1260b#	4,62	0,84			
	hsa-miR-1244	4,19	0,87			
	hsa-miR-195-3p	3,96	0,84			
	hsa-miR-1277-3p	3,91	0,88			
	hsa-miR-4454	3,57	0,84			
	hsa-miR-34c-3p	3,39	0,84			
	hsa-miR-323b-3p	3,17	0,84			
	hsa-miR-141-3p	2,84	0,89			
	hsa-miR-98-3p	2,80	0,84			
	hsa-miR-376b-3p#	2,75	0,84			
	hsa-miR-589-3p	2,61	0,89			
	hsa-miR-450a-2-3p#	2,54	0,84			
	hsa-miR-548l	2,45	0,84			
	hsa-miR-412-3p	2,37	0,84			
	hsa-let-7i-3p	2,36	0,84			
	hsa-miR-122-3p #	2,29	0,85			
	hsa-miR-34a-3p	2,28	0,84			
	hsa-miR-365a-3p	2,14	0,84			
	hsa-miR-365b-3p	2,14	0,84			
	hsa-miR-296-3p	2,06	0,90			
HD/pHD	hsa-miR-1260a	11,43	0,63	hsa-miR-184	-7,54	0,63
	hsa-miR-5100	8,80	0,63	hsa-miR-129-2-3p	-4,98	0,63
	hsa-miR-4429	6,07	0,63	hsa-miR-210-3p	-4,84	0,64
	hsa-miR-19a-3p	5,05	0,63	hsa-miR-1228-3p	-3,59	0,63
	hsa-miR-1260b	3,58	0,63	hsa-miR-940	-2,57	0,63
	hsa-miR-6529-3p	3,26	0,63	hsa-miR-500b-3p	-2,53	0,70
	hsa-miR-23c	3,13	0,63	hsa-miR-133a-3p	-2,38	0,63
	hsa-miR-122-3p	3,02	0,63	hsa-miR-30c-1-3p	-2,37	0,70
	hsa-miR-19b-3p	2,88	0,63	hsa-miR-1270	-2,33	0,70
	hsa-miR-483-3p	2,47	0,63	hsa-miR-4510	-2,28	0,66
	hsa-miR-1180-3p	2,38	0,63	hsa-miR-1304-3p	-2,15	0,63
	hsa-miR-671-3p	2,33	0,63	hsa-miR-377-3p	-2,14	0,72
	hsa-miR-1303	2,19	0,63	hsa-miR-708-3p	-2,03	0,63
	hsa-miR-26b-3p	2,16	0,63			
	hsa-miR-450a-2-3p	2,16	0,63			
	hsa-miR-376b-3p	2,12	0,63			
	hsa-miR-585-3p	2,07	0,63			
	hsa-miR-590-3p	2,02	0,63			

Data are shown as fold-change relative to control group
* Overexpressed miR in common between pHD/CTR and HD/CTR
# Overexpressed miR in common between HD/CTR and HD/pHD
$ Underexpressed miR in common between pHD/CTR and HD/CTR

To confirm the synaptic functions of the target genes we used the recently developed genomic analysis tool SynGO, a database that provides around 3000 expert-curated annotations on 1112 Synaptic Genes [62]. Among the target genes for upregulated miRNAs, several were mapped to unique SynGO annotated genes: in lines HD vs pHD, 31 of 363 genes; in lines pHD vs CTR, 25 of 276 genes; and in lines HD vs CTR, 53 of 584 genes (Supplementary Table S5). Similarly, in the target genes for downregulated miRNAs, several were mapped to unique SynGO annotated genes: in lines HD vs CTR, 65 of 751 genes; in lines HD vs pHD, 54 of 408 genes; and in lines pHD vs CTR, 167 of 1440 genes (Supplementary Table S5).

Since we exposed neuronal cultures to EVs isolated from two specific fibroblast cell lines, one control (fCTR1) and one pHD (fpHD3), we further performed a detailed analysis of the miRNAs identified in these EVs. We found 163 common miRNAs, 89 miRNAs exclusively present in the EVs from the CTR cell line, and 15 miRNAs exclusive to EVs from the pHD cell line (Figure 6A, B). Among the differentially enriched miRNAs, we found 17 upregulated and 7 downregulated in pHD vs CTR (logFC > 2 or logFC < -2, respectively) (Figure 6B; Supplementary Table S6). To gain further insight into the biological functions of the differentially enriched target genes, we performed GO enrichment analysis for biological process and pathway analysis (Supplementary Table S7). These genes were mainly involved in biological processes associated with cellular and metabolic pathways.

To better understand if these target genes were involved in synapse biology we applied, as previously, the SynGO analysis to the target genes of the downregulated miRNAs. SynGO synaptic ontology can be visualized as sunburst diagrams for synaptic location and function (Figure 6C, D). We found that 333 out of 335 are unique to SynGO annotated genes. Of these, 6 genes for cellular components and 8 for biological processes were significantly enriched at 1% FDR (Supplementary Table S6) and had functionality in synapse organization, synaptic signaling, or chemical synaptic transmission at the presynapse and postsynapse (Figure 6C, Supplementary Table S6). The SynGO analysis of the target genes for upregulated miRNAs showed that, out of 3014 genes, 310 were mapped to unique SynGO annotated genes and, of these, 6 genes for cellular components and 5 for biological processes were significantly enriched at 1% FDR (Figure 6D,

Supplementary Table S6). Functional GO enrichment analysis indicated that they were mostly involved in synapse organization, synaptic vesicle cycle, synaptic signaling, and trans-synaptic signaling, among others, at the pre and postsynaptic compartment (Figure 6D, Supplementary Table S6).

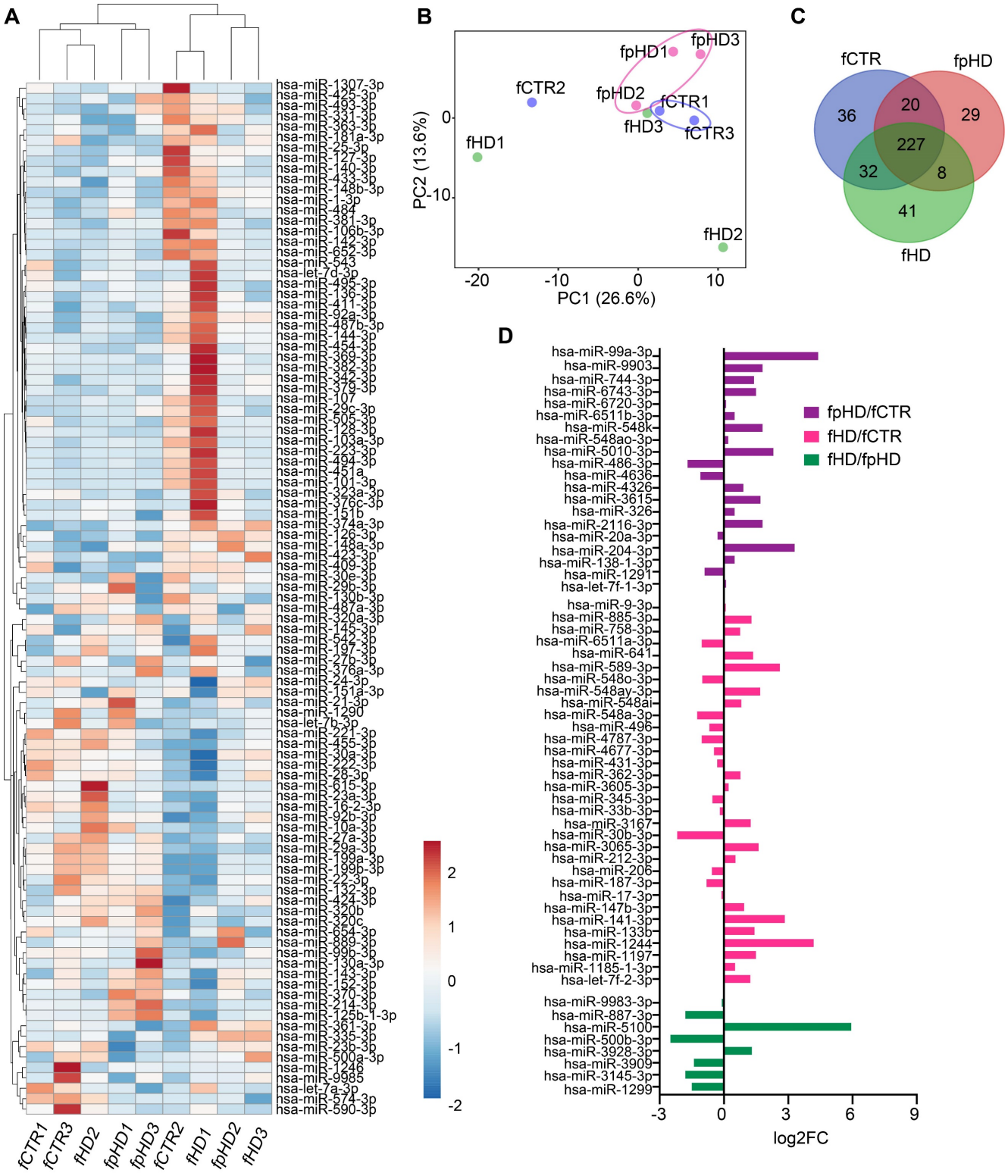

Figure 5. Characterization of miRNAs in extracellular vesicles secreted by HD and CTR fibroblasts. (A) Heatmap showing the 100 most abundant miRNAs in EVs isolated from the nine fCTR, fpHD, and fHD cell lines. High expression based on raw read counts normalized using linear transformations is shown in red while low expression is shown in blue. Rows and columns are clustered using correlation distance and average linkage; 100 rows, 9 columns. (B) PCA showing EV miRNA profiles for each group (n = 9 data points); X and Y axis show principal component 1 and principal component 2 which explain 26.6% and 13.6% of the total variance, respectively. (C) Venn diagram showing the number of miRNAs with specific expression for each group (fCTR, fpHD, and fHD lines). (D) Fold change for differentially expressed genes common to the two groups according to the Venn diagram.

Table 2. List of significantly up- and down-regulated microRNAs, or those exclusive of fpHD3- and fCTR1-derived EVs, with previously validated targets that modulate GABAergic synapses.

miRNAs	Expression	Experimentally identified targets	Involved proteins/pathways
miR-365a-3p	↑ fpHD3	↑ miR ➔ ↓GABAAR-δ (83)	GABAergic receptor
miR-195-3p	↑ fpHD3	↑ miR ➔ ↓ST6GAL1 (86)	Interplay with L1, a neural cell adhesion molecule that increases the differentiation into GABAergic neurons and the yield in mediumspiny GABAergic neurons in a HD mouse model* (87, 88)
miR-210-3p	↑ fpHD3	↑ miR ➔ ↓BDNF (85, 89)	GABAergic synapse assembly
mir-889-3p	↑ fpHD3	↑ miR ➔ ↓WNT7A (90)	GABAergic synapse assembly
miR-129-2-3p	Exclusive fpHD3	↑ miR ➔ ↓GABRA1 (84)	GABAergic receptor
miR-19a-3p	Exclusive fCTR1	↑ miR ➔ ↓TGF-β R II (91)	Removal of TGF-β R II leads to an increase in GABAergic inhibitory input to DA neurons, the ratio of inhibitory/excitatory synapses, and mIPSC frequency (92)
miR-2110	Exclusive fCTR1	↑ miR ➔ ↑Neurotensin receptor type 1 (93)	Increase in striatal GABA release (96)
miR-941	Exclusive fCTR1	↑ miR ➔ ↓ DNAJC5 (94)	GABAergic synaptic vesicles
miR-1180-3p	Exclusive fCTR1	↑ miR ➔ ↓ Dlx1 (95)	GABAergic neurogenesis

* L1 upregulates the expression of ST6GAL1 mRNA levels and L1-mediated embryonic stem cell survival is through induction of ST6GAL1 expression, making this a possible pathway that might be involved in GABAergic neurogenesis. However, to the best of our knowledge, the direct link between L1-dependent effects on the development of GABAergic neurons and ST6GAL1 has not been yet studied.

To investigate whether the list of target genes of both up- and downregulated miRNAs present in EVs that are involved in synaptic functions could be related to inhibitory synapses (GO:0060077), we compared our results with a list of validated synaptic genes predicted to be expressed in GABAergic synapses (Supplementary Table S7). We identified several genes potentially targeted by upregulated miRNAs in fpHD that are involved in postsynapse organization (N = 22; GSEA p = 0.013), regulation of postsynapse organization (N = 35; GSEA p = 0.05), regulation of translation at synapse, modulating synaptic transmission (N = 35; GSEA p = 0.08) and regulation of synapse organization (N = 7; GSEA p = 0,14) (Figure 6E, Supplementary Table S7).

To date, a few studies have been published reporting brain-specific miRNAs involved in modulating the expression of genes related to GABAergic synaptic function. We first undertook a systematic search for all published studies that identified miRNAs and gene targets that modulate GABAergic synapses and compared them to our miRNAs found in fpHD3- and fCTR1-derived EVs. We identified several dysregulated miRNAs in fpHD3 cells (vs fCTR1) that were described to disrupt GABAergic synapses, particularly by modulating $GABA_A$ receptors or assembly of synapses (Table 2). Some miRNAs were only found in a particular population, either CTR or pHD, highly suggestive of their involvement in the dysfunction of GABAergic synapses (Table 2). Taken together, these findings show that EVs secreted by cells from HD patients can carry different miRNAs than those secreted by CTR cells, the former being associated with dysregulation of synaptogenesis.

Discussion

Functional and molecular analyses of GABAergic inhibitory currents in the striatum of HD were associated with degeneration in this structure [63]. Here, we demonstrate that iPSCs reprogrammed from fibroblasts of HD patients can be differentiated into MSNs in an equivalent time course as controls, using a previously described protocol [19, 36, 38]. However, the HD-derived cell lines exhibited reduced efficiency in GABAergic striatal neuron specification, as shown by the lower levels of MAP2 and DARPP32 expression, and decreased expression of inhibitory synaptic markers in mature striatal-like neurons, associated with a delayed electrophysiological maturation phenotype. We also observed a lower whole-cell $GABA_AR$-mediated current density, mIPSC frequency, and density of GABAergic synapses in HD-derived neurons, showing dysfunction of the GABAergic system compared to CTR-derived neurons. Interestingly, while the treatment of HD-cells with EVs secreted by CTR fibroblasts restored $GABA_AR$-mediated currents and inhibitory synapse density, the incubation of CTR-derived cells with EVs from HD fibroblasts decreased both GABAR-mediated currents and GABAergic synapse density. Analysis of the miRNA content in EVs identified predicted target genes with functions at GABAergic synapses that may play a protective role through rescuing synaptic dysfunction.

Human iPSC systems for modeling HD phenotypes have provided evidence of disturbances in early developmental processes, including altered expression of genes related to neurodevelopmental pathways and synaptic homeostasis [44, 64, 65]. The HD iPSC Consortium showed that more than 50% of differentially expressed genes in HD-derived cell lines were associated with nervous system development and function. Moreover, other identified dysregulated pathways, relevant to neuronal development and maturation, included axonal guidance, Wnt signaling, Ca^{2+} signaling (voltage-gated calcium channel sub-units, plasma membrane Ca^{2+} ATPase, CAMKII, CALM), neuronal CREB signaling, and glutamate and GABA signaling [64]. Several genes with altered

expression are related to GABA synthesis, release, reuptake, or degradation, suggesting that GABAergic neurons may display increased vulnerability to mHTT cytotoxicity. A delayed electrophysiological maturation phenotype in HD iPSC-derived neurons, associated with altered developmental signatures and a reduced number of neural progenitor cells, has been reported in both monolayer neuronal cultures and 3D organoids [66-68]. Specifically, altered neuronal maturation in cultures of HD iPSC-derived striatal progenitors has been shown, with decreased levels of MAP2 compared to CTRs similar to what we observed in this work, although there was also a decreased expression of βIII-tubulin in HD-cultures vs CTR-cells contrarily to our study [66]. This discrepancy could be explained by the different time points used to assess βIII-tubulin levels. Additionally, we observed that the differentiation into MSNs was lower in HD-cultures by assessing the diminished levels of DARPP32 expression compared to CTRs, as previously demonstrated [66]. Although other authors have shown that HD striatal cultures exhibit more neuronal progenitors than CTR counterparts, they did not find lowered levels of MAP2 or DARPP32 [67]. Differentiated HD cortical MAP2$^+$ neurons have decreased neurite length and downregulation of calcium-gated channels, ultimately showcasing alterations in neuronal morphology [68]. Our data show that HD-derived iPSCs can generate electrophysiologically mature striatal-like neurons that, however, display a more depolarized resting membrane potential and greater excitability, probably due to dysfunctional inwardly rectifying K^+ channels, as also reported in other studies using HD mouse models [69, 70].

The ionotropic $GABA_A$ and glycine receptors, clustered by Gephyrin, were demonstrated to be altered in both HD mouse models and HD patients [10, 71, 72]. The underlying molecular mechanisms targeting the GABAergic system in the context of HD are still unknown, but evidence suggests that mHTT alters the transcription of genes and protein expression (e.g. $GABA_AR$ and KCC2) through interactions with transcriptional activators and repressors. However, other factors such as excitotoxicity due to impaired homeostasis of extracellular glutamate, neuroinflammation caused by the interaction of mHTT with astrocytes and microglia, and reduced GABA synthesis by astrocytes may also be involved [15, 72-75]. Additionally, $GABA_AR$ subunits (α1, α2) are specifically altered in striatal MSNs of HD mouse models R6/1 and HdhQ111 [76]. In this study, we used EVs derived from human fibroblasts to treat differentiated neuronal cultures and studied the

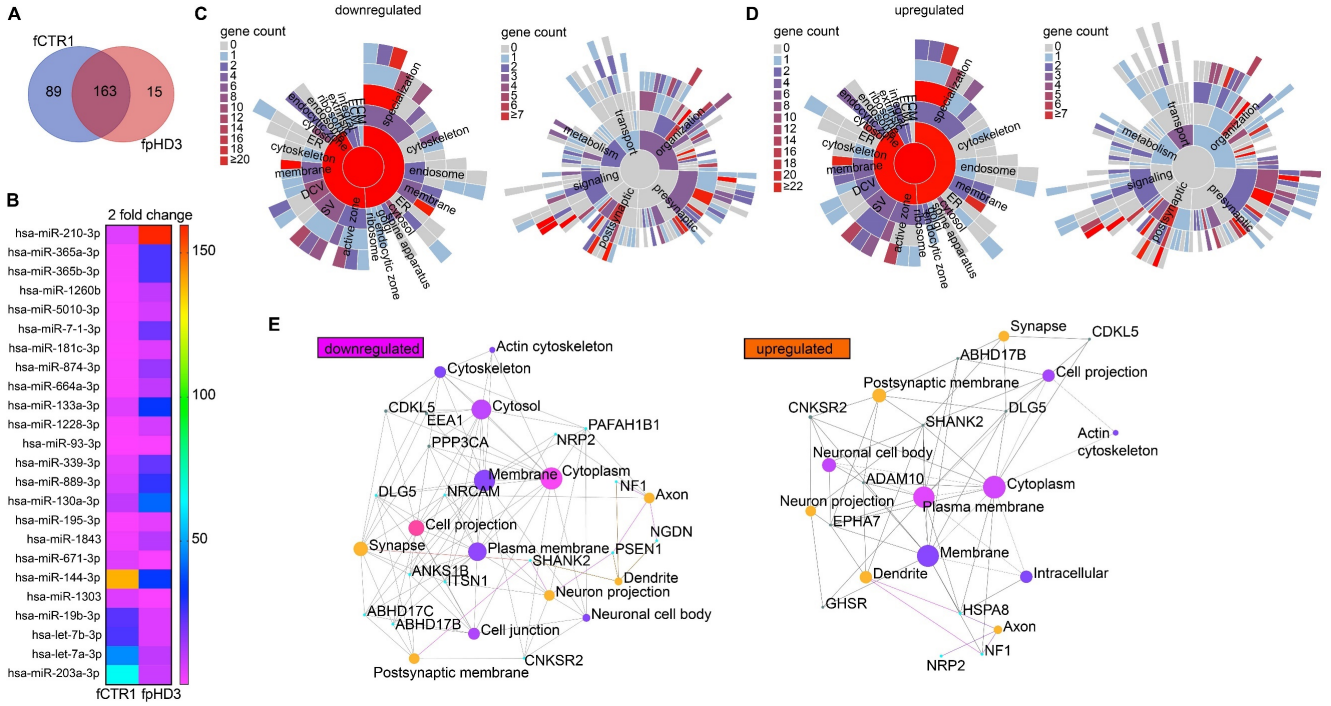

Figure 6. Identification of EV-miRNAs released from HD and CTR fibroblasts targeting genes that regulate synaptic function. (A) Venn diagram showing the number of miRNAs with specific expression in the fpHD and fCTR1 cell lines, previously shown to ameliorate abnormal GABAergic function in HD neurons. (B) Heatmap showing the expression of the EV-associated miRNA from fpHD3 and fCTR1 with a change superior to two-fold. Heatmap colors represent gene expression levels based on the provided color key scale; red for upregulated gene expression levels, and pink for downregulated gene expression levels. (C-D) SynGO Cellular Component terms and Biological Process terms are visualized in a sunburst plot for target synaptic genes of upregulated and downregulated EV miRNAs. (E) Networks of top enriched cellular components constructed by Network Analyst. Node sizes represent the enrichment significance from the Bonferroni post hoc test. The cellular components evaluated are for the set of genes associated with the ontology category GABAergic synapse (GO:0098982).

effects on GABAergic function and synaptic density. Previously, it has been demonstrated that human EVs can cross the blood-brain barrier, acting as messengers between the periphery and the central nervous system. For example, a study using blood from Parkinson's disease patients showed that EVs derived from erythrocytes can have an impact on microglia by transporting alpha-synuclein across the blood-brain barrier [77].

Here, we demonstrate that several miRNAs involved in modulating key target genes related to inhibitory synapse function are upregulated in EVs secreted by HD fibroblasts, suggesting that the functional/developmental impairment identified in neurons treated with these EVs could be, at least in part, mediated by their miRNA cargo. Several hypothetical downregulated genes that are targeted by the upregulated miRNAs identified in HD-EVs are known to regulate GABAergic synapse-related proteins (Table 2). In agreement, the metalloproteinase ADAM10 shedding enzyme, which is a known target for upregulated miRNAs found in HD-EVs, is a central protein for the development of the nervous system [78]. Indeed, the loss of ADAM10 is linked to defects in neuronal connectivity and the postnatal neuron-specific disruption of ADAM10 in the brain leads to impaired learning, defects in long-term potentiation, and seizures [79]. Another identified target was the NF1 gene, whose protein expression levels are significantly higher in inhibitory neurons than in excitatory neurons. The downregulation of NF1 expression influences both GABA concentration and $GABA_A$ receptor density, suggesting a pre- and postsynaptic mechanism [80]. Another protein that is highly expressed in GABAergic neurons is MeCP2. In MeCP2 KO mice, GABAergic synaptic transmission is strongly depressed [81] and mutations in the MeCP2 gene that cause Rett syndrome, a prevalent neurodevelopmental disorder, result in an excitatory–inhibitory imbalance [82]. Our data demonstrate that several gene candidates are predicted to affect multiple neuronal processes and contribute to reduced GABAergic synaptogenesis. Consistent with this, miRNAs identified in our study as being upregulated in HD-EVs were previously validated as targeting proteins/pathways regulating inhibitory synapses [83-85].

Our data from CTRs-EVs supports the upregulation of some particular miRNAs with previously validated targets that modulate GABAergic synapses (eg. miR-19a-3p, miR-211, miR-1180-3p, miR-941) [83-96] (Table 2). Interestingly, the cysteine string protein, encoded by the *DNAJC5* gene, resides in presynaptic terminals, clathrin-coated vesicles, and neuroendocrine secretory granules, and is involved in neurotransmitter release. Most importantly, it has been linked to Huntington's and Parkinson's diseases [97-99]. Additionally, EVs are also implicated in the development of neurodegenerative diseases, particularly proteinopathies, as they carry and spread disease-associated protein variants [20]. In accordance, our data indicate that HD-EVs carry mHTT, as previously reported [19, 29]. Our previous data have demonstrated that dysregulation of the mitochondria-lysosomal axis in HD enhances the release of EVs along with mitochondrial DNA and protein cargo [19].

In a recent study, Sharma et al. validated the role of EVs in synaptogenesis and neural circuit development and hypothesized that the effect could be mediated by the proteomic cargo of these vesicles [35]. The authors reported increased neuronal proliferation and synaptic density in human-derived differentiated neuronal cultures with MECP2 loss-of-function upon incubation with EVs from isogenic CTRs [35]. Moreover, the addition of CTR-EVs to human-derived neurospheres with MECP2 loss-of-function increased neural activity [35]. Furthermore, the injection of CTR NSC-derived EVs in a mouse model of Alzheimer's disease (AD) led to an increase in GAP43, synaptophysin, and PSD-95 synaptic markers in the cortex when compared to vehicle-injected animals [33]. In epileptic mice, the use of EVs isolated from human bone marrow-derived mesenchymal stem cells improved glutamatergic and GABAergic neurotransmission in the hippocampus [34], and mice that suffered transient ischemia showed ameliorated hippocampal long-term potentiation and synaptic transmission [32]. Moreover, the analysis of the content of stem cell-EVs (human iPSC-derived NSC and adipose-derived mesenchymal stem cells) demonstrated that these vesicles are carriers for proteins and miRNAs associated with neuroprotection and synaptogenesis, as is the case of agrin and neuroplastin; the intranasal administration of such EVs successfully led to increased hippocampal neurogenesis in WT rat and AD mouse brains, respectively [59, 100]. Our study shows that the administration of CTR-EVs might provide a therapeutic strategy to ameliorate neuronal function and synapse maintenance, specifically in early stages of HD, before a major degeneration of GABAergic neurons occurs. Understanding EV-mediated molecular mechanisms of signaling underlying this functional impact is needed to allow the exploitation of their therapeutic potential.

In conclusion, our data demonstrate for the first time that EVs from HD patient-derived fibroblasts carry bioactive molecules that have an impact on cellular functions, particularly in neurodegenerative

disease models with synaptopathy as a central feature. Additionally, the EV-mediated reversal of the pathological phenotype provides a rational basis for further studies investigating their use in therapeutic applications.

Supplementary Material

Supplementary figures and tables.
https://www.thno.org/v13p3707s1.zip

Acknowledgments

The authors acknowledge Dr. Paulo Oliveira for the critical review of the manuscript, Dr. Mónica Zuzarte for TEM analysis, and Dr. Teresa Rodrigues and Dr. Henrique Girão from the Coimbra Institute for Clinical and Biomedical Research, Faculty of Medicine, University of Coimbra, for the NTA equipment.

Funding

This work was supported by the European Regional Development Fund (ERDF), through the Centro 2020 Regional Operational Programme under project CENTRO-01-0145-FEDER-000012-Healthy Aging2020, and the COMPETE2020–Operational Programme for Competitiveness and Internationalization and Portuguese national funds via FCT-Fundação para a Ciência e a Tecnologia, under project POCI-01-0145-FEDER-029621, POCI-01-0145-FEDER-022184 and UIDB/04539/2020 and by Fundação Luso-Americana para o Desenvolvimento (FLAD) Life Science 2020 project. Paulo Pinheiro was supported by grants CEECIND/00003/2018 and CEECIND/00251/2021 from FCT.

Author contributions

Carla Lopes, and A. Cristina Rego designed this study. Margarida Beatriz, Ricardo Rodrigues, Rita Vilaça, and Carla Lopes: performed the experiments. Conceição Egas: performed RNA sequencing and analysis. Margarida Beatriz, Ricardo Rodrigues, Rita Vilaça, and Carla Lopes: analyzed the data, Carla Lopes, and Margarida Beatriz: drafted the initial manuscript. Margarida Beatriz, Ricardo Rodrigues, Rita Vilaça, Conceição Egas, Paulo Pinheiro, George Q. Daley, Thorsten M. Schlaeger, Nuno Raimundo, A. Cristina Rego, Carla Lopes: revised this manuscript. Carla Lopes: secured funding. All authors read and approved the final manuscript.

Competing Interests

The authors have declared that no competing interest exists.

References

1. MacDonald ME, Ambrose CM, Duyao MP, Myers RH, Lin C, Srinidhi L, et al. A novel gene containing a trinucleotide repeat that is expanded and unstable on Huntington's disease chromosomes. Cell. 1993;72(6):971-83.
2. Hoffner G, Island ML, Djian P. Purification of neuronal inclusions of patients with Huntington's disease reveals a broad range of N-terminal fragments of expanded huntingtin and insoluble polymers. J Neurochem. 2005;95(1):125-36.
3. Lemiere J, Decruyenaere M, Evers-Kiebooms G, Vandenbussche E, Dom R. Cognitive changes in patients with Huntington's disease (HD) and asymptomatic carriers of the HD mutation. J Neurol. 2004;251(8):935-42.
4. Beglinger LJ, O'Rourke JJF, Wang C, Langbehn DR, Duff K, Paulsen JS, et al. Earliest functional declines in Huntington disease. Psychiatry Res. 2010;178(2):414-8.
5. Thompson JC, Harris J, Sollom AC, Stopford CL, Howard E, Snowden JS, et al. Longitudinal evaluation of neuropsychiatric symptoms in Huntington's disease. J Neuropsychiatry Clin Neurosci. 2012;24(1):53-60.
6. Tabrizi SJ, Reilmann R, Roos RA, Durr A, Leavitt B, Owen G, et al. Potential endpoints for clinical trials in premanifest and early Huntington's disease in the TRACK-HD study: analysis of 24 month observational data. Lancet Neurol. 2012;11(1):42-53.
7. Paulsen JS, Long JD, Ross CA, Harrington DL, Erwin CJ, Williams JK, et al. Prediction of manifest Huntington's disease with clinical and imaging measures: a prospective observational study. Lancet Neurol. 2014;13(12):1193-201.
8. Vonsattel JPG, Keller C, del Pilar Amaya M. Neuropathology of Huntington's disease. Handb Clin Neurol. 2008;89:599-618.
9. Mehrabi NF, Waldvogel HJ, Tippett LJ, Hogg VM, Synek BJ, Faull RLM. Symptom heterogeneity in Huntington's disease correlates with neuronal degeneration in the cerebral cortex. Neurobiol Dis. 2016;96:67-74.
10. Hsu YT, Chang YG, Chern Y. Insights into GABA. Open Biol. 2018;8(12).
11. Dargaei Z, Bang JY, Mahadevan V, Khademullah CS, Bedard S, Parfitt GM, et al. Restoring GABAergic inhibition rescues memory deficits in a Huntington's disease mouse model. Proc Natl Acad Sci U S A. 2018;115(7):E1618-E26.
12. Liot G, Zala D, Pla P, Mottet G, Piel M, Saudou F. Mutant Huntingtin alters retrograde transport of TrkB receptors in striatal dendrites. J Neurosci. 2013;33(15):6298-309.
13. Ma Q, Yang J, Milner TA, Vonsattel J-PG, Palko ME, Tessarollo L, et al. SorCS2-mediated NR2A trafficking regulates motor deficits in Huntington's disease. JCI insight. 2017;2(9).
14. Twelvetrees AE, Yuen EY, Arancibia-Carcamo IL, MacAskill AF, Rostaing P, Lumb MJ, et al. Delivery of GABAARs to synapses is mediated by HAP1-KIF5 and disrupted by mutant huntingtin. Neuron. 2010;65(1):53-65.
15. Yuen EY, Wei J, Zhong P, Yan Z. Disrupted GABAAR trafficking and synaptic inhibition in a mouse model of Huntington's disease. Neurobiol Dis. 2012;46(2):497-502.
16. Pavese N, Gerhard A, Tai YF, Ho AK, Turkheimer F, Barker RA, et al. Microglial activation correlates with severity in Huntington disease: a clinical and PET study. Neurology. 2006;66(11):1638-43.
17. Spokes EGS, Garrett NJ, Rossor MN, Iversen LL. Distribution of GABA in post-mortem brain tissue from control, psychotic and Huntington's chorea subjects. J Neurol Sci. 1980;48(3):303-13.
18. Du Z, Chazalon M, Bestaven E, Leste-Lasserre T, Baufreton J, Cazalets J-R, et al. Early GABAergic transmission defects in the external globus pallidus and rest/activity rhythm alteration in a mouse model of Huntington's disease. Neuroscience. 2016;329:363-79.
19. Beatriz M, Vilaça R, Anjo SI, Manadas B, Januário C, Rego AC, et al. Defective mitochondria-lysosomal axis enhances the release of extracellular vesicles containing mitochondrial DNA and proteins in Huntington's disease. J Extracell Biol. 2022;1(10):e65.
20. Beatriz M, Vilaça R, Lopes C. Exosomes: Innocent bystanders or critical culprits in neurodegenerative diseases. Front Cell Dev Biol. 2021;9:1047.
21. Hu Z, Li Z. miRNAs in synapse development and synaptic plasticity. Curr Opin Neurobiol. 2017;45:24-31.
22. Fukuoka M, Takahashi M, Fujita H, Chiyo T, Popiel HA, Watanabe S, et al. Supplemental treatment for Huntington's disease with miR-132 that is deficient in Huntington's disease brain. Mol Ther Nucleic Acids. 2018;11:79-90.
23. Na ES, Nelson ED, Kavalali ET, Monteggia LM. The impact of MeCP2 loss-or gain-of-function on synaptic plasticity. Neuropsychopharmacology. 2013;38(1):212-9.
24. Jin J, Cheng Y, Zhang Y, Wood W, Peng Q, Hutchison E, et al. Interrogation of brain miRNA and mRNA expression profiles reveals a molecular regulatory network that is perturbed by mutant huntingtin. J Neurochem. 2012;123(4):477-90.
25. Davatolhagh MF, Fuccillo MV. Neurexin1α differentially regulates synaptic efficacy within striatal circuits. Cell Rep. 2021;34(8):108773.
26. Díez-Planelles C, Sánchez-Lozano P, Crespo MC, Gil-Zamorano J, Ribacoba R, González N, et al. Circulating microRNAs in Huntington's disease: emerging mediators in metabolic impairment. Pharmacol Res. 2016;108:102-10.
27. Martí E, Pantano L, Bañez-Coronel M, Llorens F, Miñones-Moyano E, Porta S, et al. A myriad of miRNA variants in control and Huntington's disease brain regions detected by massively parallel sequencing. Nucleic Acids Res. 2010;38(20):7219-35.

28. Reed ER, Latourelle JC, Bockholt JH, Bregu J, Smock J, Paulsen JS, et al. MicroRNAs in CSF as prodromal biomarkers for Huntington disease in the PREDICT-HD study. Neurology. 2018;90(4):e264-e72.
29. Hong Y, Zhao T, Li X-J, Li S. Mutant huntingtin inhibits αB-crystallin expression and impairs exosome secretion from astrocytes. J Neurosci. 2017;37(39):9550-63.
30. Lee M, Im W, Kim M. Exosomes as a potential messenger unit during heterochronic parabiosis for amelioration of Huntington's disease. Neurobiol Dis. 2021;155:105374.
31. Lee M, Liu T, Im W, Kim M. Exosomes from adipose-derived stem cells ameliorate phenotype of Huntington's disease in vitro model. Eur J Neurosci. 2016;44(4):2114-9.
32. Deng M, Xiao H, Zhang H, Peng H, Yuan H, Xu Y, et al. Mesenchymal stem cell-derived extracellular vesicles ameliorates hippocampal synaptic impairment after transient global ischemia. Front Cell Neurosci. 2017;11:205.
33. Li B, Liu J, Gu G, Han X, Zhang Q, Zhang W. Impact of neural stem cell-derived extracellular vesicles on mitochondrial dysfunction, sirtuin 1 level, and synaptic deficits in Alzheimer's disease. J Neurochem. 2020;154(5):502-18.
34. Long Q, Upadhya D, Hattiangady B, Kim D-K, An SY, Shuai B, et al. Intranasal MSC-derived A1-exosomes ease inflammation, and prevent abnormal neurogenesis and memory dysfunction after status epilepticus. Proc Natl Acad Sci U S A. 2017;114(17):E3536-E45.
35. Sharma P, Mesci P, Carromeu C, McClatchy DR, Schiapparelli L, Yates JR, et al. Exosomes regulate neurogenesis and circuit assembly. Proc Natl Acad Sci U S A. 2019;116(32):16086-94.
36. Lopes C, Ferreira IL, Maranga C, Beatriz M, Mota SI, Sereno J, et al. Mitochondrial and redox modifications in early stages of Huntington's disease. Redox Biol. 2022;56:102424.
37. Chambers SM, Fasano CA, Papapetrou EP, Tomishima M, Sadelain M, Studer L. Highly efficient neural conversion of human ES and iPS cells by dual inhibition of SMAD signaling. Nat Biotechnol. 2009;27(3):275-80.
38. Delli Carri A, Onorati M, Castiglioni V, Faedo A, Camnasio S, Toselli M, et al. Human pluripotent stem cell differentiation into authentic striatal projection neurons. Stem Cell Rev Rep. 2013;9(4):461-74.
39. Nicoleau C, Varela C, Bonnefond C, Maury Y, Bugi A, Aubry L, et al. Embryonic stem cells neural differentiation qualifies the role of Wnt/β-Catenin signals in human telencephalic specification and regionalization. Stem Cells. 2013;31(9):1763-74.
40. Bolte S, Cordelières FP. A guided tour into subcellular colocalization analysis in light microscopy. J Microsc. 2006;224(3):213-32.
41. Mata G, Cuesto G, Heras J, Morales M, Romero A, Rubio J, editors. SynapCountJ: a validated tool for analyzing synaptic densities in neurons 2016: Springer.
42. Evers MM, Schut MH, Pepers BA, Atalar M, van Belzen MJ, Faull RLM, et al. Making (anti-) sense out of huntingtin levels in Huntington disease. Mol Neurodegener. 2015;10(1):1-11.
43. Théry C, Amigorena S, Raposo G, Clayton A. Isolation and characterization of exosomes from cell culture supernatants and biological fluids. Curr Protoc Cell Biol. 2006;Chapter 3:Unit 3.22.
44. Lopes C, Tang Y, Anjo SI, Manadas B, Onofre I, De Almeida LP, et al. Mitochondrial and Redox Modifications in Huntington Disease Induced Pluripotent Stem Cells Rescued by CRISPR/Cas9 CAGs Targeting. Front Cell Dev Biol. 2020;8.
45. Qadir F, Aziz MA, Sari CP, Ma H, Dai H, Wang X, et al. Transcriptome reprogramming by cancer exosomes: identification of novel molecular targets in matrix and immune modulation. Mol cancer. 2018;17(1):1-16.
46. Jeon I, Cicchetti F, Cisbani G, Lee S, Li E, Bae J, et al. Human-to-mouse prion-like propagation of mutant huntingtin protein. Acta Neuropathol. 2016;132(4):577-92.
47. Tiscornia G, Singer O, Verma IM. Production and purification of lentiviral vectors. Nat protoc. 2006;1(1):241-5.
48. Bolger AM, Lohse M, Usadel B. Trimmomatic: a flexible trimmer for Illumina sequence data. Bioinformatics. 2014;30(15):2114-20.
49. Schmieder R, Edwards R. Quality control and preprocessing of metagenomic datasets. Bioinformatics. 2011;27(6):863-4.
50. Kalvari I, Nawrocki EP, Ontiveros-Palacios N, Argasinska J, Lamkiewicz K, Marz M, et al. Rfam 14: expanded coverage of metagenomic, viral and microRNA families. Nucleic Acids Res. 2021;49(D1):D192-D200.
51. Langmead B, Trapnell C, Pop M, Salzberg SL. Ultrafast and memory-efficient alignment of short DNA sequences to the human genome. Genome biol. 2009;10(3):1-10.
52. Friedländer MR, Mackowiak SD, Li N, Chen W, Rajewsky N. miRDeep2 accurately identifies known and hundreds of novel microRNA genes in seven animal clades. Nucleic Acids Res. 2012;40(1):37-52.
53. Kozomara A, Birgaoanu M, Griffiths-Jones S. miRBase: from microRNA sequences to function. Nucleic Acids Res. 2019;47(D1):D155-D62.
54. Chen Y, Wang X. miRDB: an online database for prediction of functional microRNA targets. Nucleic Acids Res. 2020;48(D1):D127-D31.
55. Xia J, Gill EE, Hancock REW. NetworkAnalyst for statistical, visual and network-based meta-analysis of gene expression data. Nat protoc. 2015;10(6):823-44.
56. Zhou G, Soufan O, Ewald J, Hancock REW, Basu N, Xia J. NetworkAnalyst 3.0: a visual analytics platform for comprehensive gene expression profiling and meta-analysis. Nucleic Acids Res. 2019;47(W1):W234-W41.
57. Koopmans F, van Nierop P, Andres-Alonso M, Byrnes A, Cijsouw T, Coba MP, et al. SynGO: An Evidence-Based, Expert-Curated Knowledge Base for the Synapse. Neuron. 2019;103(2):217-34.e4.
58. Metsalu T, Vilo J. ClustVis: a web tool for visualizing clustering of multivariate data using Principal Component Analysis and heatmap. Nucleic Acids Res. 2015;43(W1):W566-W70.
59. Upadhya R, Madhu LN, Attaluri S, Gitaí DLG, Pinson MR, Kodali M, et al. Extracellular vesicles from human iPSC-derived neural stem cells: miRNA and protein signatures, and anti-inflammatory and neurogenic properties. J Extracell Vesicles. 2020;9(1):1809064.
60. Théry C, Witwer KW, Aikawa E, Alcaraz MJ, Anderson JD, Andriantsitohaina R, et al. Minimal information for studies of extracellular vesicles 2018 (MISEV2018): a position statement of the International Society for Extracellular Vesicles and update of the MISEV2014 guidelines. J Extracell Vesicles. 2018;7(1):1535750.
61. Kuang X, Nunn K, Jiang J, Castellano P, Hardikar U, Horgan A, et al. Structural insight into transmissive mutant huntingtin species by correlative light and electron microscopy and cryo-electron tomography. Biochem Biophys Res Commun. 2021;560:99-104.
62. Koopmans F, van Nierop P, Andres-Alonso M, Byrnes A, Cijsouw T, Coba MP, et al. SynGO: an evidence-based, expert-curated knowledge base for the synapse. Neuron. 2019;103(2):217-34.
63. Garret M, Du Z, Chazalon M, Cho YH, Baufreton J. Alteration of GABA ergic neurotransmission in Huntington's disease. CNS Neurosci Ther. 2018;24(4):292-300.
64. Consortium Hi. Developmental alterations in Huntington's disease neural cells and pharmacological rescue in cells and mice. Nat Neurosci. 2017;20(5):648-60.
65. Lopes C, Aubert S, Bourgois-Rocha F, Barnat M, Rego AC, Déglon N, et al. Dominant-Negative Effects of Adult-Onset Huntingtin Mutations Alter the Division of Human Embryonic Stem Cells-Derived Neural Cells. PLoS One. 2016;11(2):e0148680.
66. Conforti P, Besusso D, Bocchi VD, Faedo A, Cesana E, Rossetti G, et al. Faulty neuronal determination and cell polarization are reverted by modulating HD early phenotypes. Proc Natl Acad Sci U S A. 2018;115(4):E762-E71.
67. Mattis VB, Tom C, Akimov S, Saeedian J, Østergaard ME, Southwell AL, et al. HD iPSC-derived neural progenitors accumulate in culture and are susceptible to BDNF withdrawal due to glutamate toxicity. Hum Mol Genet. 2015;24(11):3257-71.
68. Mehta SR, Tom CM, Wang Y, Bresee C, Rushton D, Mathkar PP, et al. Human Huntington's Disease iPSC-Derived Cortical Neurons Display Altered Transcriptomics, Morphology, and Maturation. Cell Rep. 2018;25(4):1081-96.e6.
69. Tong X, Ao Y, Faas GC, Nwaobi SE, Xu J, Haustein MD, et al. Astrocyte Kir4.1 ion channel deficits contribute to neuronal dysfunction in Huntington's disease model mice. Nat Neurosci. 2014;17(5):694-703.
70. Zhang X, Wan JQ, Tong XP. Potassium channel dysfunction in neurons and astrocytes in Huntington's disease. CNS Neurosci Ther. 2018;24(4):311-8.
71. Cepeda C, Wu N, André VM, Cummings DM, Levine MS. The corticostriatal pathway in Huntington's disease. Prog Neurobiol. 2007;81(5-6):253-71.
72. Dargaei Z, Liang X, Serranilla M, Santos J, Woodin MA. Alterations in Hippocampal Inhibitory Synaptic Transmission in the R6/2 Mouse Model of Huntington's Disease. Neuroscience. 2019;404:130-40.
73. Pribiag H, Stellwagen D. TNF-α downregulates inhibitory neurotransmission through protein phosphatase 1-dependent trafficking of GABA(A) receptors. J Neurosci. 2013;33(40):15879-93.
74. Skotte NH, Andersen JV, Santos A, Aldana BI, Willert CW, Nørremølle A, et al. Integrative Characterization of the R6/2 Mouse Model of Huntington's Disease Reveals Dysfunctional Astrocyte Metabolism. Cell Rep. 2018;23(7):2211-24.
75. Stellwagen D, Beattie EC, Seo JY, Malenka RC. Differential regulation of AMPA receptor and GABA receptor trafficking by tumor necrosis factor-alpha. J Neurosci. 2005;25(12):3219-28.
76. Du Z, Tertrais M, Courtand G, Leste-Lasserre T, Cardoit L, Masmejean F, et al. Differential alteration in expression of striatal GABAAR subunits in mouse models of Huntington's disease. Front Mol Neurosci. 2017;10:198.
77. Matsumoto J, Stewart T, Sheng L, Li N, Bullock K, Song N, et al. Transmission of α-synuclein-containing erythrocyte-derived extracellular vesicles across the blood-brain barrier via adsorptive mediated transcytosis: another mechanism for initiation and progression of Parkinson's disease? Acta Neuropathol Commun. 2017;5(1):1-16.
78. Jorissen E, Prox J, Bernreuther C, Weber S, Schwanbeck R, Serneels L, et al. The disintegrin/metalloproteinase ADAM10 is essential for the establishment of the brain cortex. J Neurosci. 2010;30(14):4833-44.
79. Kuhn P-H, Colombo AV, Schusser B, Dreymueller D, Wetzel S, Schepers U, et al. Systematic substrate identification indicates a central role for the metalloprotease ADAM10 in axon targeting and synapse function. Elife. 2016;5.
80. Violante IR, Patricio M, Bernardino I, Rebola J, Abrunhosa AJ, Ferreira N, et al. GABA deficiency in NF1: a multimodal [11C]-flumazenil and spectroscopy study. Neurology. 2016;87(9):897-904.
81. Medrihan L, Tantalaki E, Aramuni G, Sargsyan V, Dudanova I, Missler M, et al. Early defects of GABAergic synapses in the brain stem of a MeCP2 mouse model of Rett syndrome. J Neurophysiol. 2008;99(1):112-21.

82. Zhang ZW, Zak JD, Liu H. MeCP2 is required for normal development of GABAergic circuits in the thalamus. J Neurophysiol. 2010;103(5):2470-81.
83. Jovasevic V, Radulovic J. High ethanol preference and dissociated memory are co-occurring phenotypes associated with hippocampal GABA. Neurobiol Learn Mem. 2021;183:107459.
84. Wang GY, Luan ZL, Che NW, Yan DB, Sun XW, Zhang C, et al. Inhibition of microRNA-129-2-3p protects against refractory temporal lobe epilepsy by regulating GABRA1. Brain Behav. 2021;11(7):e02195.
85. Zhang S, Chen S, Liu A, Wan J, Tang L, Zheng N, et al. Inhibition of BDNF production by MPP. Neurosci Lett. 2018;675:133-9.
86. Mei J, Lin W, Li S, Tang Y, Ye Z, Lu L, et al. Long noncoding RNA TINCR facilitates hepatocellular carcinoma progression and dampens chemosensitivity to oxaliplatin by regulating the miR-195-3p/ST6GAL1/NF-κB pathway. J Exp Clin Cancer Res. 2022;41(1):1-15.
87. Li Y-L, Wu G-Z, Zeng L, Dawe GS, Sun L, Loers G, et al. Cell surface sialylation and fucosylation are regulated by the cell recognition molecule L1 via PLCγ and cooperate to modulate embryonic stem cell survival and proliferation. FEBS lett. 2009;583(4):703-10.
88. Bernreuther C, Dihné M, Johann V, Schiefer J, Cui Y, Hargus G, et al. Neural cell adhesion molecule L1-transfected embryonic stem cells promote functional recovery after excitotoxic lesion of the mouse striatum. J Neurosci. 2006;26(45):11532-9.
89. Chen X, Kong X, Niu G, Qin F, Duan Y, Ren F. Long non-coding RNA PAXIP-AS1 promotes viability, invasion, and migration of HTR-8/SVneo cells through miR-210-3p/BDNF axis. Hypertens Pregnancy. 2022;41(2):107-15.
90. Xu G, Ding Z, Shi H-f. The mechanism of miR-889 regulates osteogenesis in human bone marrow mesenchymal stem cells. J Orthop Surg Res. 2019;14(1):1-8.
91. Zou M, Wang F, Gao R, Wu J, Ou Y, Chen X, et al. Autophagy inhibition of hsa-miR-19a-3p/19b-3p by targeting TGF-β R II during TGF-β1-induced fibrogenesis in human cardiac fibroblasts. Sci Rep. 2016;6(1):1-15.
92. Luo SX, Timbang L, Kim J-I, Shang Y, Sandoval K, Tang AA, et al. TGF-β signaling in dopaminergic neurons regulates dendritic growth, excitatory-inhibitory synaptic balance, and reversal learning. Cell rep. 2016;17(12):3233-45.
93. Xiao S, Chen Y-C, Betenbaugh MJ, Martin SE, Shiloach J. MiRNA mimic screen for improved functional expression of neurotensin receptor. Biotechnol Bioeng. 2015;112(8):1632.
94. Hu HY, He L, Fominykh K, Yan Z, Guo S, Zhang X, et al. Evolution of the human-specific microRNA miR-941. Nat Commun. 2012;3(1):1-10.
95. Arcila ML, Betizeau M, Cambronne XA, Guzman E, Doerflinger N, Bouhallier F, et al. Novel primate miRNAs coevolved with ancient target genes in germinal zone-specific expression patterns. Neuron. 2014;81(6):1255-62.
96. O'Connor WT, Tanganelli S, Ungerstedt U, Fuxe K. The effects of neurotensin on GABA and acetylcholine release in the dorsal striatum of the rat: an in vivo mirodialysis study. Brain Res. 1992;573(2):209-16.
97. Ruiz R, Casanas JJ, Südhof TC, Tabares L. Cysteine string protein-α is essential for the high calcium sensitivity of exocytosis in a vertebrate synapse. Eur J Neurosci. 2008;27(12):3118-31.
98. Chandra S, Gallardo G, Fernández-Chacón R, Schlüter OM, Südhof TC. α-Synuclein cooperates with CSPα in preventing neurodegeneration. Cell. 2005;123(3):383-96.
99. Miller LC, Swayne LA, Chen L, Feng Z-P, Wacker JL, Muchowski PJ, et al. Cysteine string protein (CSP) inhibition of N-type calcium channels is blocked by mutant huntingtin. J Biol Chem. 2003;278(52):53072-81.
100. Ma X, Huang M, Zheng M, Dai C, Song Q, Zhang Q, et al. ADSCs-derived extracellular vesicles alleviate neuronal damage, promote neurogenesis and rescue memory loss in mice with Alzheimer's disease. J Control Release. 2020;327:688-702.